JOURNAL OF PETROLOGY | VOLUME 41 | NUMBER 7 | PAGES 1071–1098 | 2000

Processes in High-Mg, High-*T* Magmas: Evidence from Olivine, Chromite and Glass in Palaeogene Picrites from West Greenland

LOTTE M. LARSEN[1]* AND ASGER K. PEDERSEN[2]

[1]GEOLOGICAL SURVEY OF DENMARK AND GREENLAND, THORAVEJ 8, DK-2400 COPENHAGEN NV, DENMARK

[2]GEOLOGICAL MUSEUM, ØSTER VOLDGADE 5–7, DK-1350 COPENHAGEN K, DENMARK

RECEIVED SEPTEMBER 2, 1999; REVISED TYPESCRIPT ACCEPTED FEBRUARY 10, 2000

*Uncontaminated volcanic rocks from the 60 Ma Vaigat Formation, West Greenland, contain 6·5–30 wt % MgO, averaging 15·5 wt % MgO. Olivine (*mg*-number 77·4–93·3) forms diverse assemblages of zoned phenocrysts and xenocrysts showing evidence for equilibrium and fractional crystallization, oxidation, partial to complete re-equilibration, as well as magma mixing. The olivine crystals contain glass inclusions and have high contents of Ca and Cr, indicating that all olivines with up to* mg*-number 93·0 crystallized from melts. Associated chromites (*mg*-number 45·4–77·2) are essentially unzoned and in equilibrium with the olivines. Matrix glasses from pillow breccias have 6·7–8·8 wt % MgO and quenched close to 1200°C with oxidation states one log-unit above the NNO (nickel–nickel oxide) buffer. Compositional differences between the glasses from different volcanic members are inherited from the primary melts. The magmas erupted as crystal-charged melts, and liquids with more than ~14 wt % MgO were not erupted. The compositions of the unerupted parental melts were calculated by stepwise addition of equilibrium olivine to the matrix glasses, and these melts had 20–21 wt % MgO and liquidus temperatures of 1515–1560°C. They had lower FeO* than the erupted rocks with 20–21 wt % MgO because the rocks contain more iron-rich olivine than the melts would have had. The accumulated primary melts ascended through a lithospheric lid of ~100 km thickness, and we envisage that major crystallization took place from ~45 km depth and to the surface. Magma batches ascended in narrow dyke-like conduits and fractionated high-Mg olivine and chromite at deep levels and less magnesian crystals at shallower levels. At high ascent velocities numerous olivine crystals were carried in suspension to the surface, even some from deep levels, whereas during slower ascent most olivines settled out before eruption. Pulsating ascent rates led to mixing of magma batches in various stages of fractionation. On average, 13 wt % olivine was left within the crust, presumably as olivine-plated conduit walls. The conduit systems are similar to the crystal-rich narrow magma chambers suggested for mid-ocean ridges but are of much greater vertical extent.*

KEY WORDS: *chromite; glass; Greenland; olivine; picrite*

INTRODUCTION

Highly magnesian volcanic rocks have been used to estimate mantle melting conditions and mantle compositions because their composition may be close to that of the primary mantle-derived melts. There is, however, a long-standing discussion as to how well bulk-rock compositions actually reflect melt compositions (Drever & Johnston, 1957; Clarke, 1970; Hart & Davis, 1978, 1979; Clarke & O'Hara, 1979; Elthon & Ridley, 1979; Maaløe, 1979; Francis, 1985, 1995; Chen, 1993). Highly magnesian volcanic rocks are generally very olivine rich and may have accumulated olivine; this also applies to spinifex-textured komatiite lavas (Arndt, 1986).

Highly magnesian volcanic rocks are found in the early parts of flood basalt successions such as Karoo (Bristow, 1984; Cox *et al.*, 1984), Deccan (Krishnamurthy & Cox, 1977; Melluso *et al.*, 1995), West Greenland (Drever & Johnston, 1957; Clarke, 1970; Clarke & Pedersen, 1976) and East Greenland (Nielsen *et al.*, 1981; Fram & Lesher, 1997; Hansen & Nielsen, 1999). Assuming that these rocks represent high-Mg melts, they have been viewed

*Corresponding author. Telephone: +45-38142252. Fax: +45-38142050. E-mail: lml@geus.dk

Extended data set can be found at: http://www.petrology.oupjournals.org

as the products of partial melting in the hottest parts of mantle plumes, at temperatures considerably above normal mantle temperatures (McKenzie & Bickle, 1988; Campbell & Griffiths, 1990). The Archaean komatiites, with estimated liquid MgO contents up to 29 wt % (Nisbet *et al.*, 1993), have been taken as evidence that mantle plumes existed already in Archaean times (Campbell & Griffiths, 1992). The youngest known komatiites, the 88-my-old Gorgona komatiites, have estimated liquid MgO contents of 18–20 wt % (Aitken & Echeverria, 1984).

During continental break-up in the North Atlantic area in the Palaeogene, rifting in the Davis Strait–Baffin Bay region led to eruption of mafic and ultramafic magmas in central West Greenland and on Baffin Island [reviewed by, for example, Upton (1988) and Saunders *et al.* (1997); see also Chalmers *et al.* (1999)]. These volcanic successions contain an unusually high proportion of Mg-rich, presumably primitive high-temperature rocks (Clarke, 1970; Clarke & Pedersen, 1976). They are situated peripherally within the circular area of 2000 km diameter proposed to be influenced by the ancestral Iceland mantle plume (White & McKenzie, 1989), and this has caused debate because it is contrary to predictions from mantle plume models such as that of Campbell & Griffiths (1990), according to which Mg-rich melts should form only above the hot-spot at the centre of the plume-influenced area (Hill, 1991; Gill *et al.*, 1992).

The highly magnesian Palaeogene volcanic rocks of West Greenland contain up to 30 wt % MgO. Whereas the most magnesian rocks are probably cumulates, Clarke (1970) and Clarke & O'Hara (1979) argued that some rocks with 19–20 wt % MgO represent primary liquids. This was disputed by Hart & Davis (1978, 1979) who, on the basis of Ni partitioning between olivine and liquid, argued that rocks with more than 11–13 wt % MgO are olivine accumulative. Pedersen (1985) estimated liquid MgO contents of 18–19 wt % based on the occurrence of very magnesian olivines (up to $Fo_{92\cdot5}$). Francis (1985) produced similar estimates for the similar and coeval volcanic rocks on Baffin Island and noted that the use of bulk-rock compositions as proxies for liquid compositions requires that the phenocrysts are continuously equilibrated with the liquid. Bulk-rock compositions may indicate whether the Mg-rich members in a suite of rocks are cumulates, because if they are, the suite will in many geochemical diagrams, for example, FeO* vs MgO, form linear trends that project back to the composition of the cumulus olivine (Albarède, 1992). Individual units in the volcanic succession in West Greenland do define a number of such linear trends; these have variable slopes that project back to olivine compositions varying from Fo_{86} to Fo_{89}, suggesting the presence of accumulated olivine in some of the rocks. However, as pointed out by Hart & Davis (1979), elucidation of the true relation between rocks and liquids requires knowledge of the compositions of the phenocrysts involved. In this work, we use the compositions of olivines, chromites and glasses in the picrites of the Vaigat Formation in West Greenland to study this relation and to show how the above conundrum can be resolved. Primary high-Mg liquids did exist at depth but were not erupted; the erupted liquids had lower MgO and were charged with crystals acquired during open-system processes in the crystal-rich conduit systems during ascent to the surface.

GEOLOGICAL SETTING

The volcanic rocks in the West Greenland Basin cover onshore areas of $\sim$22 000 km^2 mainly on Disko island, Nuussuaq peninsula and Svartenhuk Halvø (Clarke & Pedersen, 1976), and an even larger submerged area on the shelf (e.g. Escher & Pulvertaft, 1995; Chalmers *et al.*, 1999). The overall vertical thickness of the exposed volcanic succession is 2–3 km on Disko and Nuussuaq but because the depocentres shifted laterally with time the stratigraphic thicknesses are considerably higher. In all the onshore areas the volcanic succession can be divided into a lower part with Mg-rich olivine-phyric rocks (the Vaigat Formation) and an upper part with plagioclase-phyric rocks that have been assigned to a number of local formations. The Vaigat Formation constitutes roughly one-third of the erupted volume.

The Paleocene volcanic succession on Disko and Nuussuaq has been dated at 60·7 $\pm$ 0·5 to 59·4 $\pm$ 0·5 Ma (Storey *et al.*, 1998). There are no discernible age differences within the Vaigat Formation, which was probably erupted within around half a million years with very high eruption rates.

Vaigat Formation

The Mg-rich rocks of the Vaigat Formation form a widespread series of light grey, thin pahoehoe lava flows and hyaloclastite breccias. Vertical thicknesses reach $\sim$1800 m. Subordinate intercalated horizons of brownish, aphyric, less-magnesian rocks, enriched in silica, are interpreted to have resulted from reaction between mafic magmas and crustal rocks, often in high-level magma chambers within the underlying sedimentary succession (Pedersen, 1979*a*, 1985; Pedersen & Pedersen, 1987; Goodrich & Patchett, 1991; Lightfoot *et al.*, 1997). The contaminated rocks are not considered further in this paper, which is solely concerned with the uncontaminated parts of the Vaigat Formation.

The volcanism of the Vaigat Formation occurred in three main cycles, which are represented by the three main members. These are, from older to younger, the Anaanaa

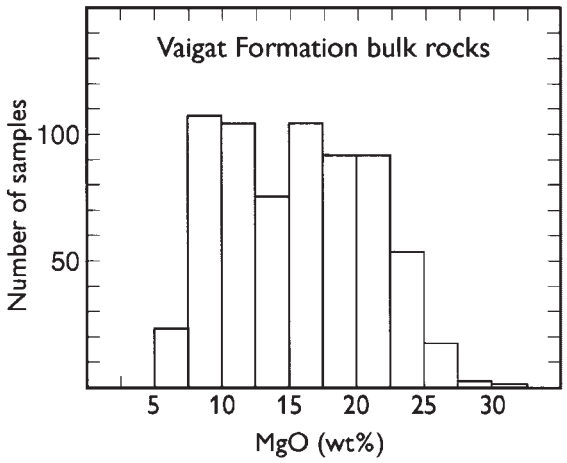

Fig. 1. Frequency distribution of MgO contents in 665 bulk-rock samples of the Vaigat Formation, calculated volatile-free. The average MgO content is 15·5 wt %, and 451 samples (68%) have MgO >12 wt % and conform to the definition of picrite by Le Bas *et al.* (2000). The distribution only approximately reflects the real volume relations because some volcanic units with 5–10 wt % MgO are oversampled.

Member, Naujánguit Member and Ordlingassoq Member. Each cycle started with olivine-rich magmas and ended with more evolved, often contaminated magmas. At the initiation of the volcanism the environment was a sea-covered shelf, and after build-up to above sea level the volcanic pile prograded eastwards into the sea and gradually filled the basin (Pedersen *et al.*, 1993, 1996; Pedersen *et al.*, 1998). Because of the progradational deposition, hyaloclastite breccias formed in abundance during all three cycles, often by entry of subaerial lava flows into water.

The uncontaminated rocks of the Vaigat Formation contain 6·5–30 wt % MgO with an average of 15·5 wt % MgO (Fig. 1). Following the IUGS nomenclature (Le Bas *et al.*, 2000) the majority of the rocks are picrites (MgO >12 wt %), and the remaining rocks are basalts. All the rocks are tholeiitic.

PETROGRAPHY AND MINERALOGY

The majority of the uncontaminated rocks of the Vaigat Formation have olivine and chromite as the only phenocryst phases. The most magnesian rocks have abundant equant to prismatic phenocrysts of olivine up to 3–4 mm in size, and chromite up to 0·1 mm in size (Figs 2 and 3). With declining content of MgO in the rock the phenocrysts become smaller. In rocks with less than ~15 wt % MgO most olivines are <1 mm in size and the rocks are olivine microphyric or aphyric in hand sample. Rocks with <9 wt % MgO are aphyric or olivine–plagioclase phyric. Rocks with plagioclase phenocrysts are rare in the Vaigat Formation. Glassy rocks have phenocrysts of equant to elongate–skeletal olivine with included or attached chromites set in clear pale yellow glass (Fig. 2a and b; Fig. 3), sometimes with plagioclase microlites. The rare evolved rocks also have plagioclase glomerocrysts in the glass. The glassy rocks typically consist of ~70% glass and 30% crystals; no glassy rocks are truly aphyric.

Groundmass minerals are plagioclase, olivine, clinopyroxene and Fe–Ti oxides. Pillows from pillow breccias have chilled glass rims of 0·5–1 cm width and interiors with aphanitic to intersertal textures (Fig. 2a and b). Groundmasses in lava flows are variably fine-grained intersertal, coarse-grained subophitic, or intergranular. Although the crystalline groundmasses frequently contain abundant elongate–skeletal olivine crystals (Fig. 2c) and sometimes show feathery quench textures, spinifex textures have not been observed. Vesicle fillings and alteration minerals include various zeolites and Ca-hydrosilicates, clays, carbonate and silica phases.

Microprobe analyses of phenocrysts, glass inclusions and matrix glasses were made on a JEOL Superprobe at the University of Copenhagen, using either wavelength-dispersive (WDS) or energy-dispersive (EDS) analytical systems, and a combination of natural and synthetic standards. Normal operating conditions were 15 kV accelerating voltage, 15 nA beam current, 20 s total counting time for WDS and 60 s lifetime for EDS analyses. High-precision analyses of the minor elements Ca, Cr, Ni and Ti in olivine and Ni, Ti and V in chromite were made using 100 nA beam current and 40 s total counting time (WDS); the lower limits of detection for these conditions are 15–30 ppm (Pedersen, 1985, p. 35). Tiny glass inclusions in olivine were analysed with 2 nA beam current (EDS) to minimize volatilization during analysis. Data on the tabulated samples are given in the Appendix. Large datasets for olivines, chromites and glasses are given as supplementary data on the *Journal of Petrology* web site, at http://www.petrology.oupjournals.org.

Olivine

The olivines are texturally complex (Fig. 3), and several types of olivine are found within a single sample. Crystals of all types may contain scattered inclusions of glass and chromite.

The most frequent olivines are equant to somewhat elongated, clear euhedral to subhedral crystals of all sizes (Fig. 3a, b and d). The larger crystals often form clusters of several individuals. Strained, kink-banded crystals are occasionally observed but are rare. Some crystals have rounded or embayed outlines and may enclose patches of groundmass, making them more or less skeletal. Following Drever & Johnston (1957) and Donaldson (1976) this is

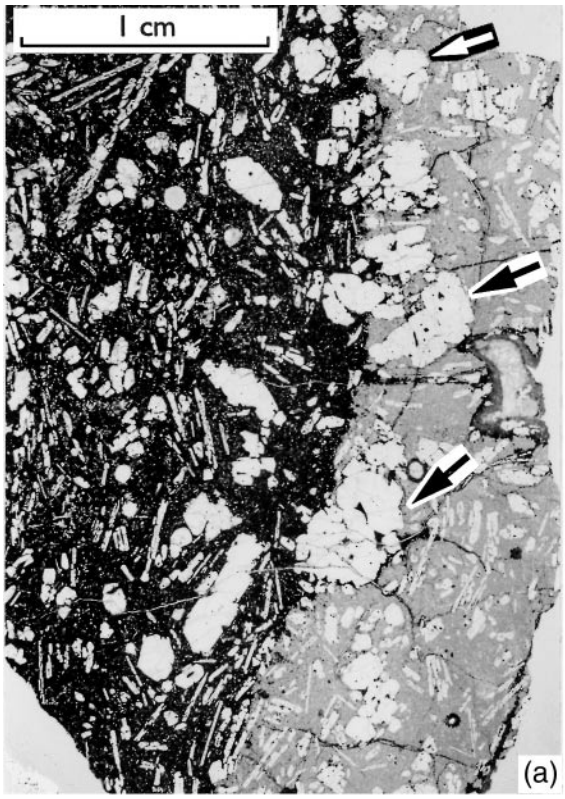
1 cm
(a)

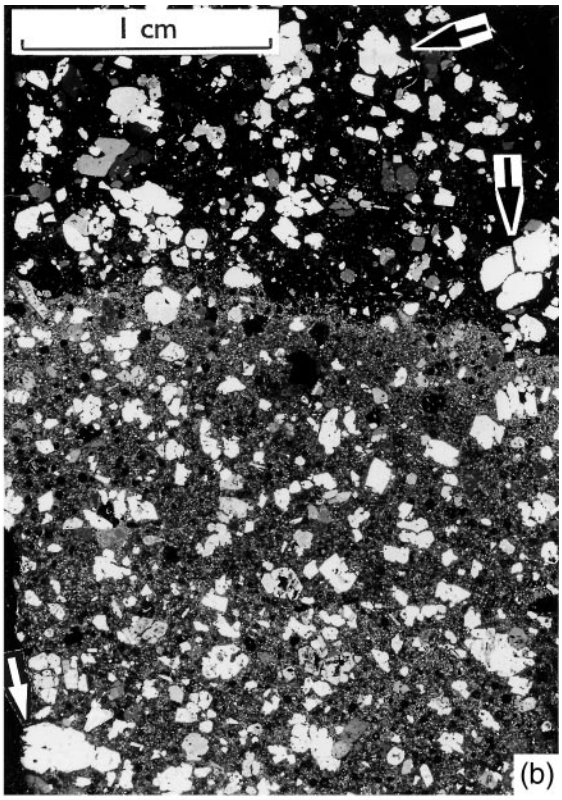
1 cm
(b)

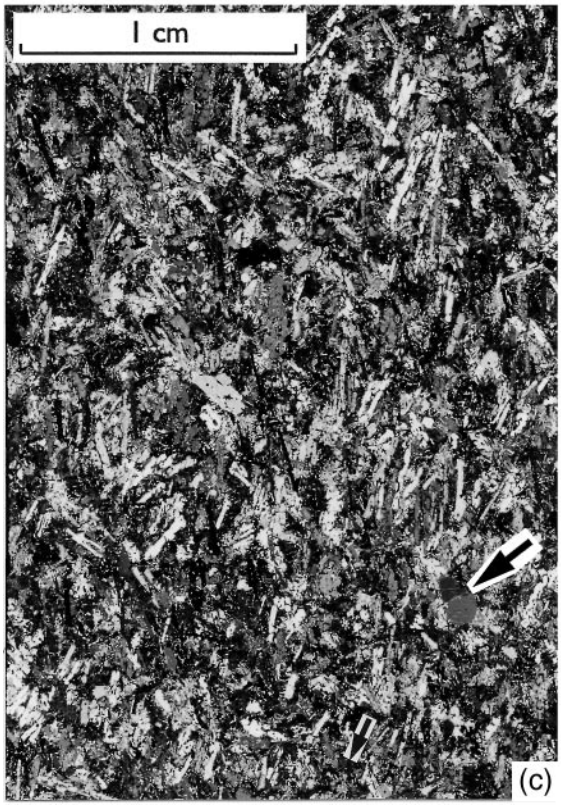
1 cm
(c)

interpreted as a result of rapid primary growth and generally not as a result of resorption. The morphological types described by Donaldson (1976) as hopper olivine are frequently observed.

Some olivine crystals have inclusion-filled zones ('necklaces') separating the crystals into cores with rounded outlines and rims (Fig. 3e). The compositional zoning continues with little or no interruption across the inclusion zone.

Other olivine crystals have dark, dusty cores crowded with tiny inclusions (often below microprobe resolution) of oxide and glass (Fig. 3b, f and g). Such inclusion-filled cores may be either euhedral or rounded, and they are surrounded by clear rims. Cores of this type show some within-grain compositional variability, partly but not completely because of variable success in avoiding the inclusions during microprobe analysis. The compositional range is mostly within the range of the clear olivines, and the clear rims are of normal groundmass composition. A few such inclusion-filled crystals or clusters are found in more than half of all thin sections.

Rare anhedral olivines have broken or ragged outlines and may be overgrown with a fringe of small olivine crystals (Fig. 3c and d). Reverse compositional zoning confirms the xenocrystic nature of these crystals.

Quenched olivine crystals may be tiny and near-equant hoppers (Fig. 2b) but are often elongated up to 8 mm long and 0·5 mm wide, and skeletal to highly skeletal, consisting of parallel-set rods and blebs in optical continuity (chain and parallel-growth olivines, Donaldson, 1976) (Fig. 2a).

Complex olivine populations similar to those in the Vaigat Formation have been described from Hawaii by, for example, Maaløe & Hansen (1982), Helz (1987), Baker *et al.* (1996) and Garcia (1996), one difference being the scarcity of kink-banded olivine in the Vaigat Formation. Drever & Johnston (1957) discussed and illustrated many of the same features in olivines from the Vaigat Formation on Ubekendt Ejland, West Greenland, north of Nuussuaq.

Olivine compositions

Representative olivine compositions are given in Table 1. The olivines are denoted by their *mg*-number, i.e. atomic 100Mg/(Mg + Fe). The Vaigat Formation olivines span the compositional range *mg*-number 76·5–93·3, with the major part of the analyses in the range *mg*-number 85–89 (Fig. 4). Around half of the samples with microprobed phenocrysts contain olivines with very Mg-rich cores with *mg*-number >90 (see Appendix). These crystals are always near-equant and usually (but not always) among the larger crystals in a section (Fig. 2); they are mostly undeformed and contain inclusions of chromite and glass (Fig. 3h). They are visually indistinguishable from similar olivine crystals with *mg*-number <90. The Mg-rich olivines normally constitute <1% of a thin section, and in the histogram (Fig. 4) they are overrepresented because they were searched for.

Olivines with *mg*-number >90 are a common feature of komatiites (Arndt *et al.*, 1977; Nisbet *et al.*, 1977; Echeverria, 1980; Lesher, 1989) and are also reported from magnesian lavas in arc settings (e.g. Eggins, 1993; Kamenetsky *et al.*, 1995*a*, 1995*b*). They are only rarely reported from mid-ocean ridge basalt (MORB) (Donaldson & Brown, 1977; Kamenetsky *et al.*, 1998), ocean island basalt (OIB) or continental basalts. Olivines with up to *mg*-number 93 have been described from the picrites on Baffin Island (Francis, 1985; Kent *et al.*, 1998). On Hawaii, the well-analysed olivine populations do not exceed *mg*-number 90·7 (Maaløe & Hansen, 1982; Yang *et al.*, 1994; Baker *et al.*, 1996; Garcia, 1996), and crystals with *mg*-number >90 appear to be very rare.

The olivines of the Vaigat Formation contain significant amounts of the minor elements Ca, Cr and Ni. There is a very good correlation between the contents of these elements and the *mg*-number of the olivine, with Ca increasing and Cr and Ni decreasing with decreasing *mg*-number (Fig. 5). The Mg-rich olivines with *mg*-number >90 contain 0·23–0·35 wt % CaO and 0·09–0·19 wt % Cr_2O_3. Together with the glass inclusions this clearly shows that the Mg-rich

Fig. 2. Thin sections of picrites from West Greenland. (a) Pillow rim with glassy crust (right) and dark aphanitic interior (left). Equant to elongated phenocrysts of olivine in single crystals and clusters. Skeletal rods of quench olivine with chain and parallel-growth morphologies (Donaldson, 1976) indicating high cooling rates and high degrees of supercooling. The wide size range of both equant and skeletal olivines should be noted (NB: the rock contains no plagioclase). White arrow points to cluster of Mg-rich olivines (*mg*-number up to 92·8), and black arrows point to clusters of olivines with *mg*-number up to 90·5 and 88·8. Bulk-rock MgO = 21·6 wt %. GGU 400452, plane-polarized light. (b) Pillow rim with glassy crust (glass at top, isotropic) and aphanitic interior. Near-equant olivine crystals ranging in size down to groundmass. Many crystals have hopper morphologies with embayments and hollow cores; no elongate chain olivines are developed, indicating lower cooling rates and degrees of supercooling than in (a). White arrow points to cluster of Mg-rich olivines (*mg*-number up to 93·1), and black arrows point to clusters of olivines with *mg*-number up to 87·7 and 87·2. Bulk-rock MgO = 19·9 wt %. GGU 362148, crossed polars. (c) Lava with crystalline groundmass. Numerous flow-aligned very elongated skeletal olivine crystals up to 5 mm long, many with linked parallel-growth morphology indicating high cooling rates (Donaldson, 1976). The matrix consists of ophitically intergrown clinopyroxene and plagioclase and microcrystalline areas of oxide-rich mesostasis. Black arrow points to a single equant olivine crystal with *mg*-number 90·9. The quench olivines have *mg*-number 89·7–81·4. Bulk-rock MgO = 18·2 wt %. GGU 400299, crossed polars.

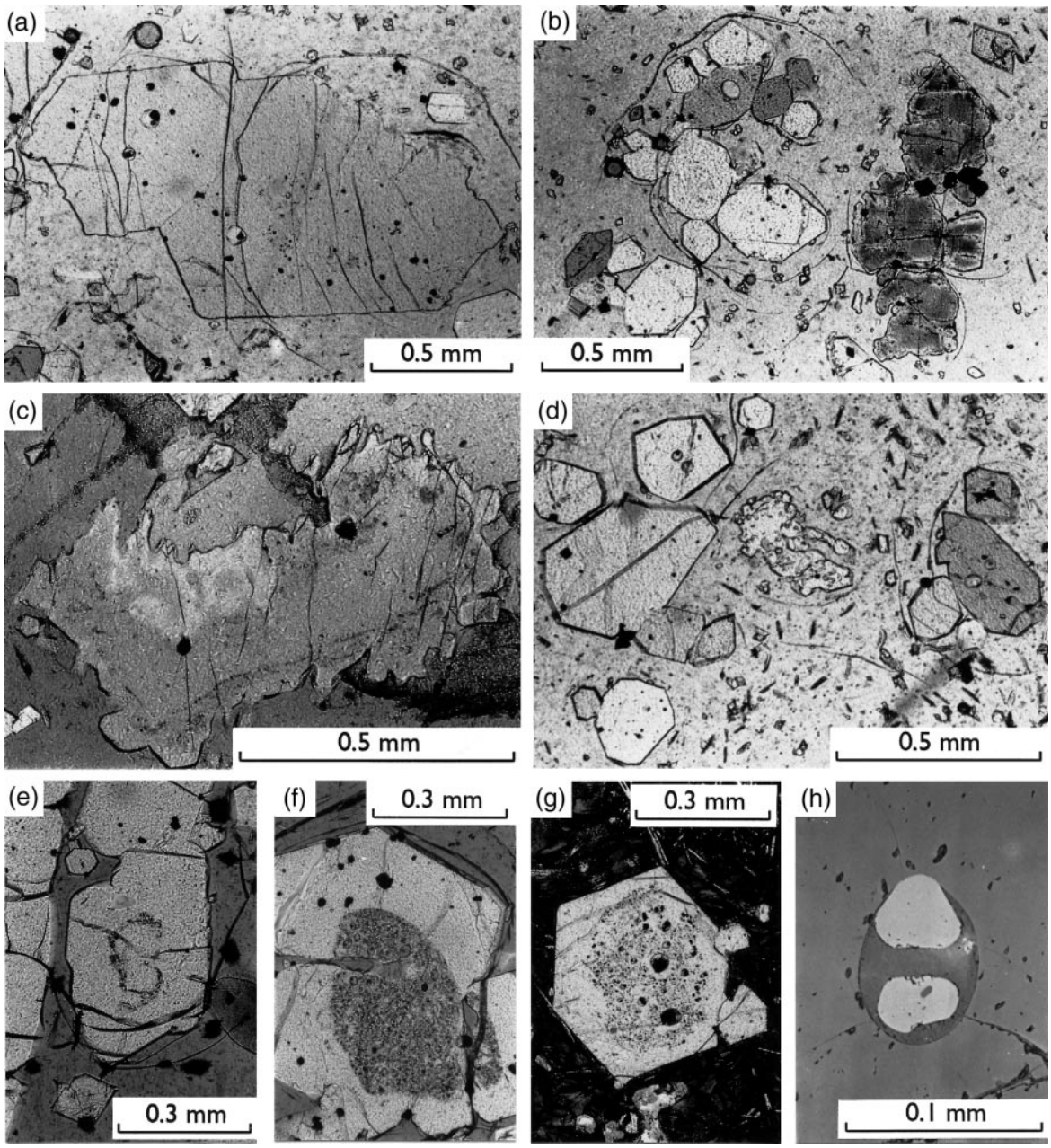

Fig. 3. Olivine textures. (a) Euhedral olivine phenocryst with somewhat lobate outline in upper right part. The crystal is zoned from *mg*-number 90·2 in the centre to *mg*-number 84·5 in a marginal zone, reversed to *mg*-number 85·1 in the outermost rim (Table 1, nos 23–27; Fig. 7). It contains inclusions of chromite and glass up to 70 μm (Table 4). Matrix is clear glass with small euhedral olivine crystals. GGU 136943, plane-polarized light. (b) Loose cluster of clear euhedral olivine phenocrysts (cores *mg*-number 88·3 to rims *mg*-number 86·4) juxtaposed to a cluster of olivines (in optical continuity) densely speckled with tiny dark inclusions (olivine cores *mg*-number 88·5 to rims *mg*-number 86·4), set in clear glass matrix with tiny olivines. GGU 136943, plane-polarized light. (c) Irregular, highly resorbed and regrown olivine crystal, reversely zoned from *mg*-number 84·7 in the core to *mg*-number 85·3 in the rim. Matrix glass is patchily altered. GGU 327100, partly crossed polars. (d) Strongly resorbed, spongy olivine grain, *mg*-number 78·3–84·8, among euhedral olivine phenocrysts in clear glass with plagioclase microlites. GGU 136943, plane-polarized light. (e) Subhedral olivine phenocryst with interior inclusion zone ('necklace'), *mg*-number 88·4 in centre, *mg*-number 88·6 in rim, in clear glass matrix. GGU 264137, partly crossed polars. (f) Euhedral olivine phenocryst with a rounded dark core crowded with inclusions of glass and oxides, in clear glass matrix. (Note tube-like glass-filled channel stretching into the crystal centre from the left side.) Not analysed. GGU 264104, partly crossed polars. (g) Euhedral olivine crystal with rounded core with numerous glass and chromite inclusions up to 40 μm in size. Olivine *mg*-number 88·1 in core and 87·3 in clear rim. Black aphanitic matrix with plagioclase microlites. GGU 136943, plane-polarized light. (h) Euhedral to rounded chromite crystals within a large glass inclusion in olivine phenocryst *mg*-number 92·2. Chromite analysis in Table 2, no. 5. The glass is altered to clay, probably because it is crossed by a crack. GGU 136943, reflected light.

Table 1: Olivines from the Vaigat Formation, West Greenland

Analysis:	1	2	3	4	5	6	7	8	9	10	11	12	13	14	15	16	17	18
SiO_2	40·80	40·73	40·75	40·05	39·90	41·44	41·03	40·75	40·95	40·43	40·71	39·86	39·90	39·34	41·57	41·29	40·31	40·16
TiO_2	0·01	0·01	0·01	0·01	0·01	0·01	0·01	0·01	0·01	0·01	0·01	0·01	0·01	0·01	0·01	0·01	0·01	0·01
Cr_2O_3	0·145	0·135	0·090	0·097	0·064	0·154	0·168	0·111	0·093	0·062	0·123	0·048	0·031	0·028	0·131	0·104	0·088	0·097
FeO	7·41	8·03	9·20	11·76	12·93	7·47	7·87	9·49	10·79	12·68	8·01	13·05	11·03	12·76	6·97	7·50	11·03	11·87
MnO	0·20	0·19	0·14	0·20	0·32	0·15	0·14	0·14	0·14	0·20	0·16	0·28	0·16	0·18	0·14	0·14	0·15	0·16
MgO	51·12	49·73	49·13	46·74	45·90	50·84	50·54	49·53	48·05	46·84	50·01	45·58	46·34	45·18	50·59	50·09	46·61	46·39
NiO	0·447	0·397	0·452	0·353	0·302	0·433	0·449	0·438	0·394	0·337	0·438	0·317	0·289	0·317	0·425	0·446	0·384	0·392
CaO	0·309	0·317	0·277	0·345	0·346	0·293	0·304	0·310	0·294	0·361	0·282	0·346	0·380	0·446	0·310	0·265	0·332	0·298
Sum	100·44	99·54	100·05	99·56	99·77	100·79	100·51	100·78	100·72	100·92	99·74	99·49	98·14	98·26	100·15	99·85	98·91	99·38
mg-no.	92·48	91·69	90·49	87·63	86·35	92·38	91·96	90·29	88·81	86·81	91·75	86·16	88·22	86·32	92·82	92·25	88·28	87·44

Analysis:	19	20	21	22	23	24	25	26	27	28	29	30	31	32	33	34	35	36
SiO_2	40·41	40·84	41·02	40·79	40·67	40·30	40·12	39·61	39·55	39·78	40·34	40·01	39·69	40·68	40·35	40·02	40·09	39·80
TiO_2	0·01	0·01	0·003	0·007	0·006	0·012	0·010	0·008	0·014	0·015	0·012	0·023	0·030	0·013	0·010	0·010	0·023	0·013
Cr_2O_3	0·080	0·045	0·127	0·157	0·085	0·084	0·060	0·063	0·035	0·096	0·058	0·158	0·039	0·111	0·074	0·047	0·033	0·062
FeO	13·29	8·90	7·64	8·65	9·44	10·13	11·57	14·47	13·93	11·04	10·88	11·14	14·28	9·05	10·88	14·43	13·96	13·02
MnO	0·18	0·35	0·114	0·130	0·146	0·149	0·166	0·228	0·244	0·178	0·195	0·168	0·215	0·124	0·150	0·225	0·211	0·190
MgO	46·05	48·52	50·37	49·43	48·62	47·95	46·75	44·42	44·60	46·55	47·12	46·29	44·58	49·15	47·38	44·98	45·49	46·20
NiO	0·343	0·300	0·456	0·451	0·423	0·409	0·395	0·338	0·281	0·364	0·300	0·310	0·211	0·408	0·354	0·307	0·276	0·325
CaO	0·373	0·450	0·270	0·266	0·258	0·254	0·252	0·293	0·276	0·309	0·382	0·290	0·313	0·285	0·383	0·306	0·348	0·344
Sum	100·74	99·42	100·00	99·88	99·65	99·29	99·32	99·43	98·93	98·33	99·29	98·39	99·36	99·82	99·58	100·32	100·43	99·95
mg-no.	86·06	90·67	92·16	91·06	90·17	89·40	87·80	84·54	85·09	88·25	88·53	88·10	84·76	90·63	88·58	84·74	85·31	86·34

Elements in wt % oxides. Values for TiO_2, Cr_2O_3, MnO, NiO and CaO with three decimal places were obtained with trace element analytical technique (see text). *mg*-number is atomic 100 Mg/(Mg + Fe). Petrographic notes: 1–5, GGU 400452. 1–2, centre and margin of large olivine crystal (white arrow in Fig. 2a; cross-section in Fig. 6b); 3–4, centres of large olivine crystals (black arrows in Fig. 2a); 5, small equant olivine crystal, rim towards groundmass glass. 6–14, GGU 332771. 6–10, large olivine crystal in cluster, traverse from centre to rim (cross-section in Fig. 6c), high-Cr crystal (Fig. 7b); 11 and 12, centre and rim of another olivine crystal in the same cluster, lower Cr contents (Fig. 7b); 13 and 14, dusty, speckled olivine crystal (13, light patch; 14, dark patch; note low Cr and high Ca in both). 15–20, GGU 362148. 15–17, centre, margin and rim of large olivine crystal in cluster (white arrow in Fig. 2b, cross-section in Fig. 6a); 18 and 19, centre and rim of large olivine crystal (lower black arrow in Fig. 2b, cross-section in Fig. 6d); 20, centre of small dark dusty olivine crystal (note low Cr and high Ca). 21–31, GGU 136943. 21 and 22, centre and outer centre of large olivine crystal, relatively high Cr (Fig. 7a); 23–27, traverse from centre to rim of olivine crystal shown in Fig. 3a (note reverse zoning in outermost rim); low-Cr, low-Ca crystal (Fig. 7a); 28 and 29, centres of clear (28) and dark dusty (29) olivine crystals shown in Fig. 3b; 30, centre of inclusion-filled olivine crystal shown in Fig. 3g; 31, irregular iron-rich olivine xenocryst shown in Fig. 3d. 32–35, GGU 327100. 32, margin of large olivine crystal; 33, centre of small olivine crystal; 34 and 35, centre and overgrowth of anhedral olivine xenocryst shown in Fig. 3c (note reverse zoning). 36, GGU 264217. Olivine from rock with completely re-equilibrated olivine population (Fig. 7c).

olivines crystallized from melts. They are not xenocrysts of mantle olivines, which have very low contents of Ca and Cr (Fig. 5; Gurenko *et al.*, 1996). Further, the smooth and continuous trends through the whole olivine compositional range shown in Fig. 5 strongly suggest that the Mg-rich olivine crystals are cognate phenocrysts and not accidental xenocrysts.

Olivine zoning

Most olivine phenocrysts are normally zoned with steepening or linear compositional gradients towards the margins (Fig. 6a–d); most of the larger cores have compositions of *mg*-number 87–89. Even the skeletal quench olivines are normally zoned (Fig. 6e). In the glassy rocks the most iron-rich olivine rims bordering the matrix glass have compositions of *mg*-number 82–85, whereas more iron-rich rims occur in the crystalline lava samples. The Mg-rich olivines (*mg*-number >90) differ from the other olivines in having cores with constant composition and normally zoned rims, giving flat-topped compositional profiles (Fig. 6a and b). The significance of the different zoning profiles in Fig. 6 is discussed later in the section on phenocryst–melt relations. In a few samples the olivines are unzoned with all compositions within a narrow interval around *mg*-number 86–87, even

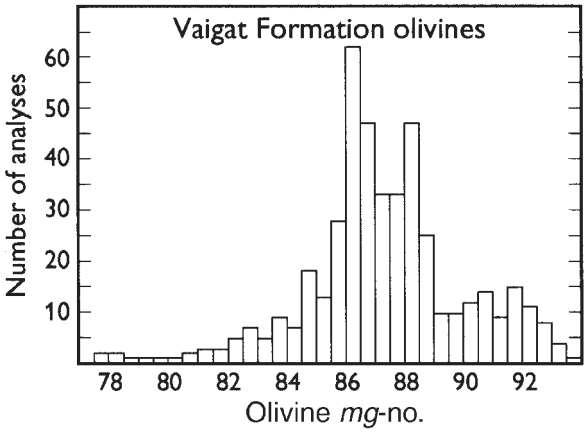

Fig. 4. Histogram of all olivine analyses (418) from the Vaigat Formation. *mg*-number is atomic 100Mg/(Mg + Fe). Olivines with *mg*-number >90 are overrepresented because they were searched for; they normally constitute <1% of a thin section.

though these rocks show exactly the same petrographic diversity of the olivines as other samples.

Olivine crystals even within the same sample have individual zoning trends with respect to the minor elements: for the same *mg*-numbers the crystals have different levels of Ca, Cr and Ni (Fig. 7). A few normally zoned crystals have thin reversely zoned rims. The petrographically identified xenocrysts have outlying compositions and are often reversely zoned. The different levels of minor elements suggest that olivine crystals within the same sample did not crystallize from completely identical melts, as discussed later.

Chromite

Chromite forms euhedral to rounded crystals most frequently 10–50 μm in size, enclosed in or attached to olivine, and sometimes also 'free' in the matrix glass (Fig. 3). The crystals enclosed in olivine are unzoned or slightly zoned, but individual crystals differ somewhat in composition from one host olivine to the other. The chromite crystals enclosed in matrix glass may show more pronounced zoning and in some cases signs of oxidation and re-equilibration along the rims.

Chromite compositions

Representative chromite analyses are given in Table 2. The compositional range encountered in unaltered chromites is *mg*-number 45·4–77·2, *cr*-number 44·9–69·5. TiO_2 is <1 wt % in the primary chromites but may be up to 3 wt % in re-equilibrated rims. There is a positive correlation between *mg*-number in coexisting olivine and chromite (Fig. 8). The chromites enclosed in olivine with *mg*-number >90 form a distinct high-Mg group with more Mg and less Fe^{2+}, and more Al + Cr and less Fe^{3+}, than the other chromites (Fig. 9). The major substitutions from the high-Mg group to the main group are Mg → Fe^{2+}, (Al + Cr) → Fe^{3+} and Al ↔ Cr. The high-Mg chromites have unusually low contents of total iron (FeO* = 12–20 wt %). They have somewhat lower Fe^{3+}/Fe^{2+} ratios than the main group of chromites although the intervals overlap. In a plot of *cr*-number in

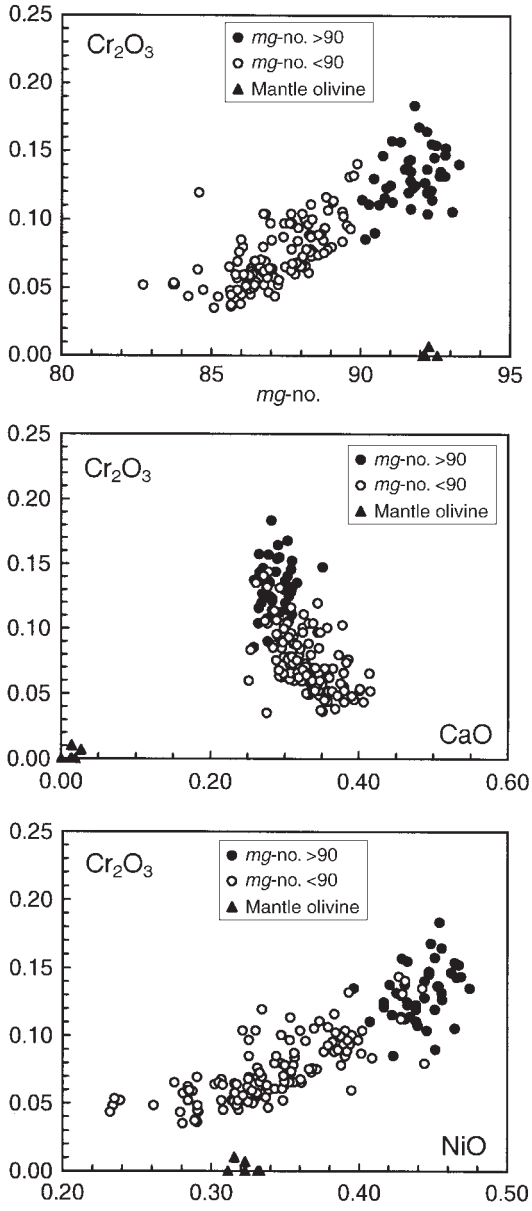

Fig. 5. Minor elements (wt % oxides) in Vaigat Formation olivines, high-precision microprobe analyses only. Olivine xenocrysts scatter somewhat in these plots and are not shown. For comparison, mantle olivines (from a West Grenland lherzolite xenolith) analysed simultaneously are also shown: in contrast to the igneous olivines the mantle olivines have very low CaO and Cr_2O_3.

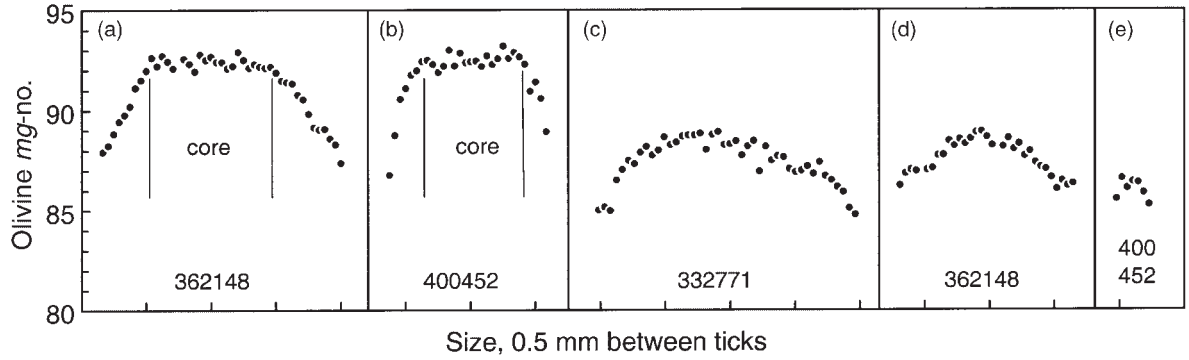

Fig. 6. Microprobe traverses across olivine crystals. (a–d) large, clear, euhedral to subhedral phenocrysts. Noteworthy features are the flat-topped zoning profiles in (a) and (b), crystal rims with curved zoning profiles in (b) and (c), and rims with linear zoning profiles in (a) and (d) (from the same sample). (e) Section across an elongate, skeletal quench crystal, which is also zoned. (See text for discussion.)

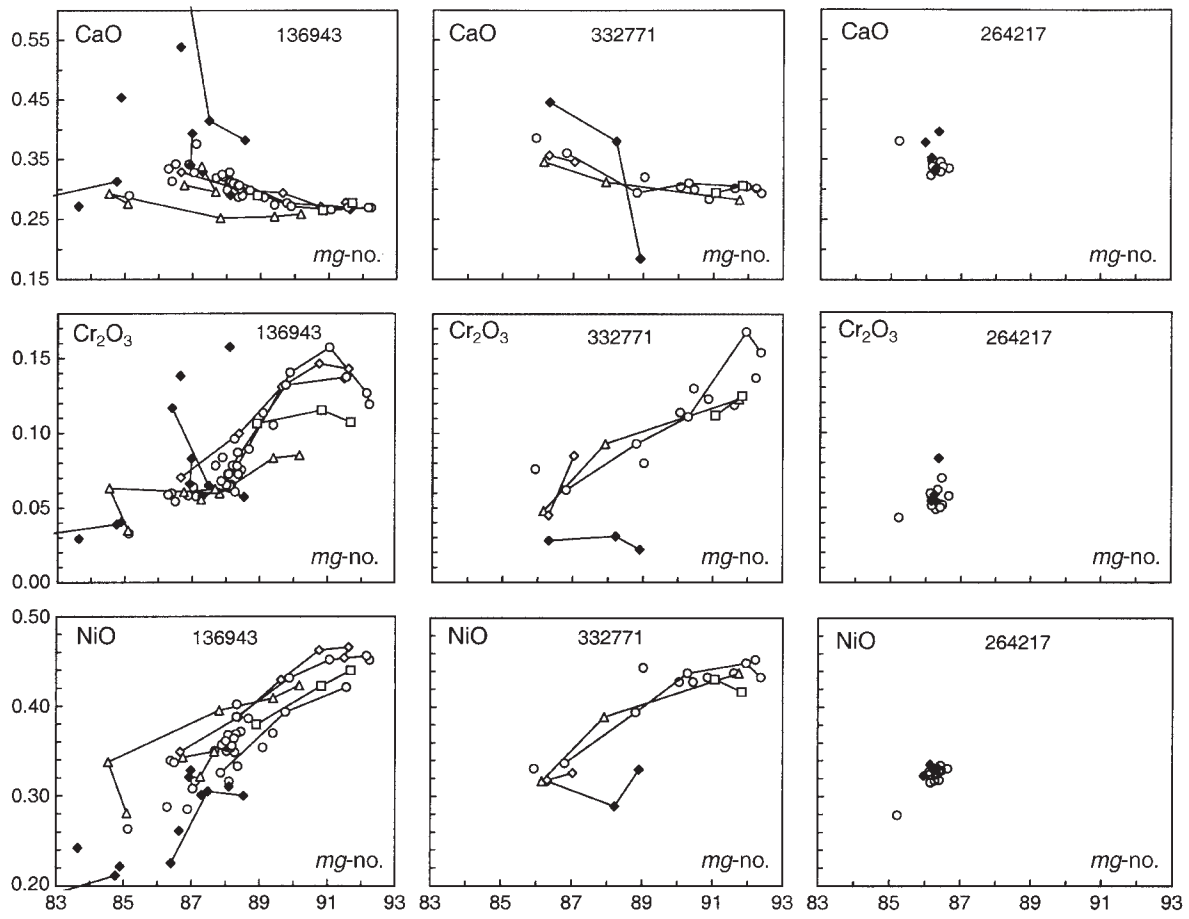

Fig. 7. Zoning trends for the minor elements CaO, Cr_2O_3 and NiO (wt %) in olivines. Analysis points in individual crystals are connected by lines. Different open symbols help to distinguish trends in individual phenocrysts within a sample; filled diamonds are xenocrysts that often have high CaO. (Note individual concentration levels in each crystal.) Sample 136943 shows distinct differences in individual zoning trends. Sample 332771 shows less inter-crystal differences. Sample 264217 has an olivine assemblage that is petrographically just as diverse as in the other samples, but almost all crystals are re-equilibrated to *mg*-number 86·2 ± 0·3 (1σ, 17 analyses); two xenocrysts and a late groundmass crystal are different.

Table 2: Chromites from the Vaigat Formation, West Greenland

Analysis:	1	2	3	4	5	6	7	8	9	10	11	12
Sample:	400452	332771	362148	327100	136943	136943	136943	400450	136943	136943	400450	136943
SiO_2	0·01	0·01	0·01	0·13	0·13	0·16	0·15	0·01	0·11	0·17	0·01	0·13
TiO_2	0·47	0·23	0·85	0·96	0·55	0·50	0·33	0·43	0·74	0·61	0·39	0·60
Al_2O_3	22·71	18·27	22·50	22·18	19·58	19·08	15·16	20·77	14·86	22·62	18·46	20·99
Cr_2O_3	44·36	48·68	45·20	41·71	47·73	48·17	51·50	43·16	45·04	38·24	44·87	38·93
V_2O_3	n.a.	n.a.	n.a.	0·13	0·11	0·08	0·07	n.a.	0·09	0·15	n.a.	0·13
Fe_2O_3	4·49	4·64	3·73	7·69	5·21	5·36	6·09	7·31	11·58	9·84	7·51	10·35
FeO	11·00	11·71	10·20	10·97	10·23	10·32	12·23	12·42	12·05	13·15	14·45	15·56
MnO	0·20	0·22	0·24	0·17	0·16	0·18	0·19	0·20	0·18	0·19	0·19	0·22
MgO	15·97	14·76	16·65	16·38	16·33	16·17	14·45	14·73	14·51	14·61	13·15	12·91
NiO	0·19	0·16	0·33	0·28	0·26	0·25	0·22	0·24	0·26	0·24	0·23	0·20
CaO	0·05	0·04	0·01	0·00	0·00	0·00	0·00	0·08	0·11	0·00	0·07	0·00
Sum	99·45	98·72	99·72	100·60	100·29	100·27	100·39	99·35	99·53	99·82	99·33	100·02
FeO*	15·04	15·88	13·56	17·89	14·92	15·15	17·71	19·00	22·47	22·00	21·21	24·88
Recalculation based on 24 cations and 32 oxygens												
Ti	0·09	0·04	0·15	0·17	0·10	0·09	0·06	0·08	0·14	0·11	0·07	0·11
Al	6·50	5·40	6·40	6·30	5·63	5·50	4·49	6·05	4·45	6·53	5·49	6·16
Cr	8·51	9·64	8·62	7·94	9·20	9·31	10·22	8·43	9·04	7·40	8·94	7·66
V				0·03	0·02	0·02	0·01		0·02	0·03		0·03
Fe^{3+}	0·82	0·88	0·68	1·39	0·96	0·99	1·15	1·36	2·21	1·81	1·42	1·94
Fe^{2+}	2·23	2·45	2·06	2·21	2·08	2·11	2·57	2·57	2·56	2·69	3·05	3·24
Mn	0·04	0·05	0·05	0·03	0·03	0·04	0·04	0·04	0·04	0·04	0·04	0·05
Mg	5·78	5·51	5·98	5·88	5·93	5·89	5·41	5·42	5·49	5·33	4·94	4·79
Ni	0·04	0·03	0·06	0·05	0·05	0·05	0·04	0·05	0·05	0·05	0·05	0·04
mg-no.	72·13	69·2	74·42	72·69	73·99	73·63	67·79	67·88	68·2	66·45	61·85	59·65
cr-no.	56·71	64·12	57·39	55·77	62·05	62·87	69·49	58·22	67·02	53·13	61·98	55·43
fe-no.	5·18	5·53	4·33	8·89	6·08	6·27	7·25	8·59	14·08	11·50	8·96	12·31
$Fe^{3+}/\Sigma Fe$	0·27	0·26	0·25	0·39	0·32	0·32	0·31	0·35	0·46	0·40	0·32	0·37
Coexisting olivines												
mg-no.	92·5	91·6	92·8	90·6	92·2	91·6	91·1	89·7	89·4	88·2	87·7	87·0
Table 1	1		15	32	21		22		24			

chromite vs *mg*-number in coexisting olivine (Fig. 8) the high-Mg chromites fall within the array for mantle spinels defined by Arai (1994*a*, 1994*b*), whereas the main group of chromites fall outside the mantle array at near-constant *cr*-number, the fractional crystallization trend of Dick & Bullen (1984) and Arai (1994*b*).

The main group of chromites are broadly similar to some Cr-spinels from MORBs (Dick & Bullen, 1984; Allan, 1992, 1994). They have higher *cr*-number than spinels from most abyssal peridotites and fall on an extension of Dick & Bullen's (1984) abyssal peridotite trend. The high-Mg chromites plot on the high-temperature side of the abyssal peridotite trend, suggesting very high crystallization temperatures.

The high-Mg chromites do not have many counterparts in the literature. Chromites from the Gorgona komatiites (Echeverria, 1980) are broadly similar. In Archaean komatiites, most chromites have higher Fe and Cr and lower Mg and Al (Arndt *et al.*, 1977; Nisbet *et al.*, 1977; Lesher, 1989). The chromite populations from Belingwe and Mt Keith extend to Mg-rich and Fe-poor compositions similar to the high-Mg chromites in West Greenland (Zhou & Kerrich, 1992; Barnes, 1998). However, the high-Mg chromites from Belingwe have much higher *cr*-numbers whereas those from Mt Keith have lower *fe*-numbers. Chromites included in olivine *mg*-number >90 from Vulsini have similar Fe and Mg but higher Cr and lower Al (Kamenetsky *et al.*, 1995*a*). Some of the best

Analysis	13	14	15	16	17	18	19	20	21	22	23	24
Sample:	400452	332771	362148	327100	136943	136943	136943	136943	136943	136943	327100	400493
SiO_2	0·01	0·01	0·01	0·21	0·15	0·00	0·14	0·15	0·14	0·15	0·17	0·14
TiO_2	0·57	0·83	0·85	0·90	0·87	1·03	0·93	0·93	3·86	0·69	1·24	1·00
Al_2O_3	21·39	21·35	23·94	18·65	24·42	21·40	20·71	7·90	18·95	16·35	20·32	23·02
Cr_2O_3	37·72	37·47	37·17	38·29	34·04	38·10	40·28	21·99	33·51	45·83	30·83	35·84
V_2O_3	n.a.	n.a.	n.a.	0·15	0·12	0·18	0·21	0·07	0·76	0·16	0·21	n.a.
Fe_2O_3	10·47	11·02	8·01	12·82	10·65	11·11	9·19	40·92	11·63	8·54	18·19	9·15
FeO	15·40	16·22	14·96	16·51	13·68	15·21	13·19	17·43	14·84	15·42	16·10	16·53
MnO	0·34	0·19	0·26	0·22	0·16	0·40	0·25	0·20	0·22	0·14	0·22	0·49
MgO	12·71	12·66	13·54	12·25	14·40	13·70	14·56	10·22	14·81	12·69	12·83	12·25
NiO	0·25	0·24	0·23	0·14	0·22	0·00	0·17	0·24	0·29	0·18	0·23	0·23
CaO	0·05	0·01	0·07	0·00	0·00	0·38	0·00	0·05	0·00	0·05	0·00	0·26
Sum	98·91	100·00	99·04	100·14	98·71	101·51	99·63	100·10	99·01	100·20	100·34	98·91
FeO*	24·82	26·14	22·17	28·05	23·26	25·20	21·46	54·25	25·30	23·10	32·47	24·76
Recalculation based on 24 cations and 32 oxygens												
Ti	0·11	0·15	0·16	0·17	0·16	0·19	0·17	0·19	0·73	0·13	0·23	0·19
Al	6·33	6·26	6·96	5·55	7·07	6·17	6·03	2·53	5·58	4·89	5·98	6·80
Cr	7·48	7·37	7·24	7·64	6·61	7·37	7·87	4·72	6·62	9·19	6·09	7·10
V				0·03	0·02	0·04	0·04	0·02	0·15	0·03	0·04	
Fe^{3+}	1·98	2·06	1·49	2·44	1·97	2·04	1·71	8·36	2·19	1·63	3·42	1·72
Fe^{2+}	3·23	3·38	3·08	3·49	2·81	3·11	2·73	3·96	3·10	3·27	3·36	3·46
Mn	0·07	0·04	0·05	0·05	0·03	0·08	0·05	0·05	0·05	0·03	0·05	0·10
Mg	4·75	4·69	4·97	4·61	5·27	5·00	5·36	4·13	5·52	4·80	4·78	4·57
Ni	0·05	0·05	0·05	0·03	0·04	0·00	0·03	0·05	0·06	0·04	0·05	0·05
mg-no.	59·52	58·17	61·73	56·93	65·23	61·62	66·29	51·1	64·01	59·46	58·68	56·91
cr-no.	54·18	54·06	51·01	57·93	48·31	54·42	56·6	65·11	54·25	65·27	50·43	51·08
fe-no.	12·54	13·13	9·50	15·61	12·59	13·09	10·95	53·56	15·22	10·38	22·08	11·01
$Fe^{3+}/\Sigma Fe$	0·38	0·38	0·33	0·41	0·41	0·40	0·39	0·68	0·41	0·33	0·50	0·33
Coexisting olivines												
mg-no.	85·8	86·0	(86·6)	(86·0)	(86·9)	(86·5)	88·5	88·1	87·8	85·4	84·7	(84·0)
Table 1							29				34	

Analyses in wt % oxides. n.a., not analysed; FeO*, total iron as FeO; *mg*-number is atomic 100 Mg/(Mg + Fe^{2+}); *cr*-number is atomic 100 Cr/(Cr + Al); *fe*-number atomic 100 Fe^{3+}/(Cr + Al + Fe^{3+}). Petrographic notes: 1–7, euhedral to rounded chromites in olivine cores with *mg*-number >90. Number 5 is shown in Fig. 3h. 8–12, euhedral to rounded chromites in olivine cores with *mg*-number 87–90. 13–18, chromites and Cr-spinels in olivine rims with *mg*-number <87 (13–14) and in glass (15–18). Olivine *mg*-numbers in parentheses are estimated. 19–23, Cr-spinel xenocrysts or in xenocrystic olivine. 19, chromite in dark, dusty olivine crystal (Fig. 3b); 20, chromian magnesio-ferrite in oxidized olivine grain; 21, re-equilibrated chromite in oxidized olivine; 22, irregular chromite xenocryst fringed by olivine, in glass; 23, oxidized Cr-spinel in olivine xenocryst (Fig. 3c); 24, chromite in plagioclase phenocryst An_{86}.

analogues from natural rocks are chromites from harzburgites (Haggerty, 1976, 1991; Arai, 1994*b*; Allan & Dick, 1996; Bernstein *et al.*, 1998), which might suggest that the primary melts left a harzburgitic residue. It is, however, improbable that the Vaigat Formation chromites are un-equilibrated restites from mantle melting. Some of them are euhedral crystals sitting in melt inclusions within the Mg-rich olivines (Fig. 3h).

The very wide range of *mg*-number in the chromites from West Greenland is matched only by chromites in komatiites (Barnes, 1998). Likewise, the only matching experimental chromites are those formed by melting experiments on a komatiite from Kambalda (Murck & Campbell, 1986). In Fig. 10 the West Greenland and the experimental chromites are compared. The Mg and Fe^{2+} variations, which are temperature dependent, are

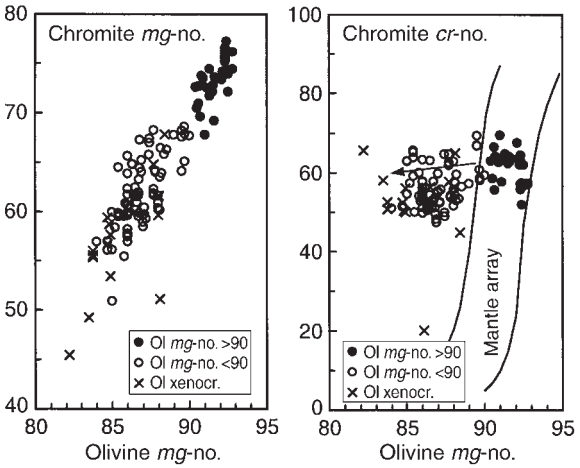

Fig. 8. Compositions of coexisting chromites and olivines in the Vaigat Formation. *mg*-number = atomic 100Mg/(Mg + Fe^{2+}), *cr*-number = atomic 100Cr/(Cr + Al). The two parallel curves in the *cr*-number diagram delineate the array of mantle spinels defined by Arai (1994*a*, 1994*b*). Fractional crystallization trends run from the mantle array towards lower *mg*-number, as indicated by an arrow.

similar, especially considering that the lowest crystallization temperatures for the West Greenland chromites are around 1200°C (see later) compared with 1300°C as the lowest for the Kambalda experiments. High-Mg chromites and olivines with *mg*-number >90 formed in the experiments at temperatures of 1350–1500°C in equilibrium with melts with 18·2–25·6 wt % MgO, and similar conditions are expected to apply for the West Greenland magmas. However, Cr and Al behave differently in the high-temperature ends in Fig. 10. In the 1 atm experiments, rising temperature leads to uniformly increasing Cr and decreasing Al. The two Greenland examples behave like the experiments with rising temperature (increasing olivine *mg*-number) only up to a certain level (olivine *mg*-number 91 and 88) above which Cr decreases and Al increases. We suspect that this is an effect of pressure, the high-Mg olivines and enclosed chromites having crystallized at considerable depths.

Glass

Matrix glasses

The fresh glass in the samples is pale yellow and transparent, and often shows curved fractures (Fig. 3a–d). Incipient devitrification is seen as dark brown feathery patches, and alteration to green clay is often concentrated in and around vesicles.

The compositions of representative matrix glasses and their corresponding bulk rocks are presented in Table 3 and plotted in Fig. 11. The analytical totals of the fresh glasses are in the range 97·5–100·2% (average 98·8%), indicating that the glasses are not significantly hydrated. Separated glasses have contents of H_2O + CO_2 in the range 0·15–0·37 wt %. Within any sample the matrix glass is fairly homogeneous. The glasses span a relatively narrow range of MgO contents, 7·5–8·8 wt % for the olivine-phyric rocks and 7·1–7·6 wt % for the plagioclase-phyric rocks. There is a wider relative range in FeO*, 9·4–11·6 wt %, and an even larger relative range in TiO_2, 1·3–1·9 wt %. The compositional ranges of TiO_2 and FeO* in the glasses reflect corresponding ranges in the bulk rocks, as shown by the near-parallel glass–bulk-rock tie-lines in Fig. 11: the most Ti- and Fe-rich bulk rocks also have the most Ti- and Fe-rich glasses, and the

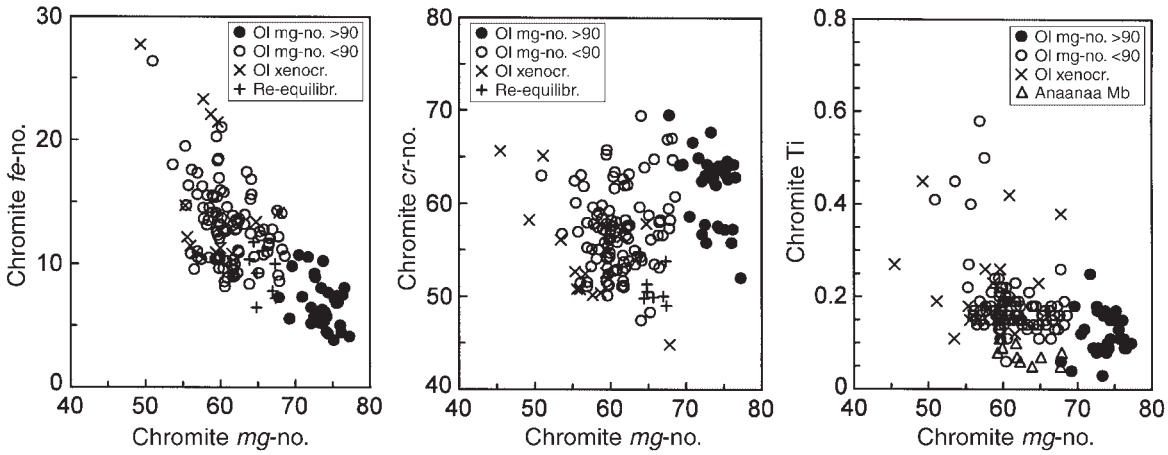

Fig. 9. Chromite compositional variations. *mg*-number and *cr*-number as in Fig. 8; *fe*-number = atomic 100Fe^{3+}/(Fe^{3+} + Al + Cr); Ti = atoms per 24 cations. The scatter in these diagrams is caused by several factors: chromites from different samples show different levels of *fe*-number, *cr*-number and Ti (especially clearly seen for *cr*-number and low Ti in Anaanaa Mb); fractionation trends follow different directions and may change direction (see Fig. 10); re-equilibration lowers *cr*-number and *fe*-number; many xenocrysts have outlying compositions.

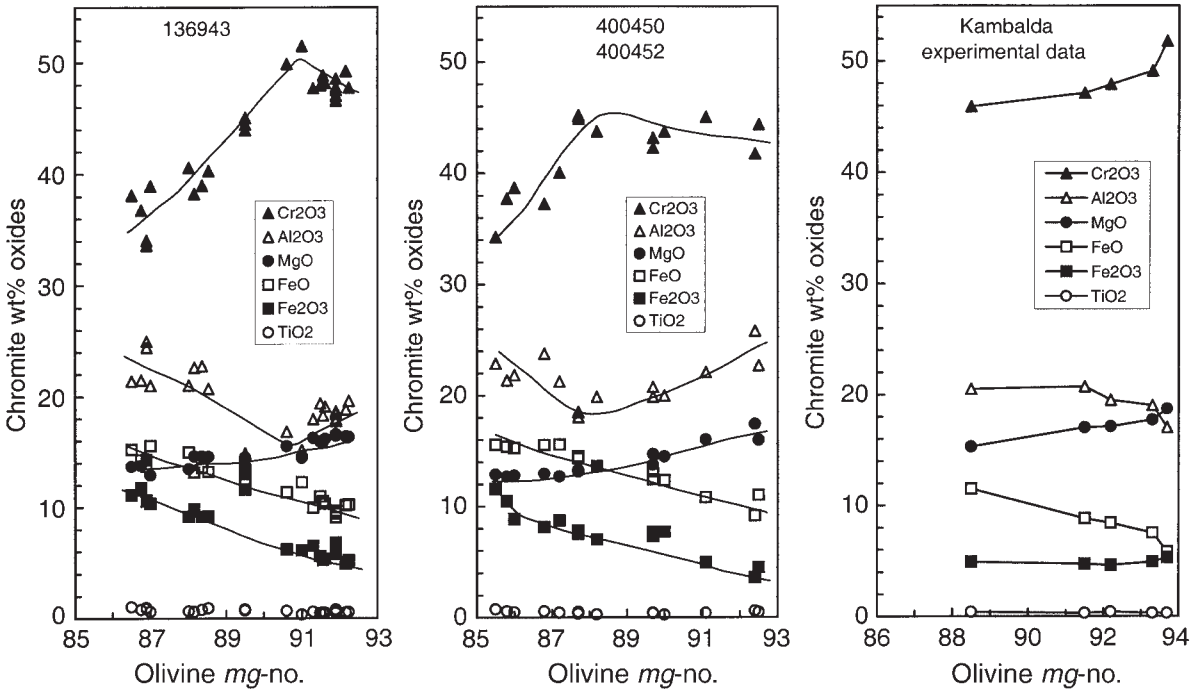

Fig. 10. Chromite compositions vs olivine *mg*-number (xenocrysts excluded) in some Vaigat Formation samples (400450 and 400452 are closely related) compared with experimental chromites and olivines from the Kambalda komatiite (Murck & Campbell, 1986). The experiments were performed at 1 atm pressure, fO_2 = FMQ, and T = 1300°C–1500°C, with 50°C between experiments. Olivine *mg*-number is a proxy for crystallization temperature, and the Vaigat Formation chromites crystallized to lower temperatures (1200°C) than the Kambalda chromites. (See text for discussion.)

tie-lines simply reflect the presence of olivine in the bulk rocks. The compositional ranges in TiO_2 and FeO* in the glasses and bulk rocks must reflect similar ranges in the primary mantle melts.

The CaO contents in the glasses are high, 12·5–14·0 wt % CaO, as expected after prolonged olivine crystallization. The reason for the quenching of the melts within a narrow interval of MgO is probably the approach of plagioclase saturation. The steep trends defined by the glasses in Fig. 11 are interpreted as olivine–plagioclase cotectics (Francis, 1985), which the olivine-fractionating liquids reached along the individual liquid lines of descent. Only the plagioclase-phyric melts have started to move along the cotectic trend with steep TiO_2 and FeO* enrichment. The plagioclase-phyric melts have precipitated plagioclase of composition $An_{88–74}$.

Glass inclusions

The olivine phenocrysts contain glass inclusions, which have been analysed in four samples (Table 4). The inclusions are rounded or elongate, up to 70 μm in size, and sometimes contain a shrinkage bubble. Most inclusions contain a euhedral to rounded chromite crystal (Fig. 3h), which, because of its size, must have been present before the entrapment. It appears that many glass inclusions were formed in connection with inclusion of a chromite crystal into the growing olivine.

In contrast to the homogeneous matrix glasses the inclusion glasses show considerable compositional variation, with MgO = 3·0–8·7 wt %, FeO* = 4·2–9·3 wt %, and SiO_2 = 49·1–55·0 wt %. They have high CaO (12·6–15·5 wt %) and Al_2O_3 (13·9–17·8 wt %), with CaO/Al_2O_3 ratios fairly constant around 0·80–0·90. Compositional variability of glass inclusions in contrast to matrix glasses seems to be a common phenomenon (Sobolev & Shimizu, 1994; Kamenetsky *et al.*, 1995*a*, 1998; Gurenko *et al.*, 1996; Kent *et al.*, 1998). It has been ascribed partly to initial melt differences and partly to post-entrapment modification of the inclusions. Post-entrapment modification arises through two processes: (1) precipitation of olivine from the melt onto the inclusion walls; (2) diffusional homogenization of the olivine, with diffusion of Fe from the more Fe-rich olivine of the precipitated inclusion rim into the mass of the host olivine, and ensuing re-equilibration of the trapped melt (Gurenko *et al.*, 1996). By these processes the glass inclusion loses Fe to the large reservoir of the host olivine, and the lost Fe is not available for dissolution back into the inclusion during high-T homogenization experiments. Therefore both homogenized and unhomogenized glass

Table 3: Pillow glasses and corresponding bulk rocks from the Vaigat Formation, West Greenland

	Anaanaa Member			Naujánguit Member					Ordlingassoq Member					
Sample:	400450	400452	400493	176712	264217	264219	332771	362148	136943	156737	264099	264105	264137	327100
Glasses														
SiO_2	48·61	48·42	49·36	47·87	48·51	48·59	48·42	48·53	47·72	48·99	48·49	48·75	48·48	47·55
TiO_2	1·77	1·38	1·69	1·58	1·46	1·47	1·52	1·57	1·60	1·90	1·86	1·78	1·61	1·78
Al_2O_3	13·85	13·99	13·48	14·20	15·03	14·54	13·76	14·26	15·11	14·14	14·51	14·53	15·05	14·88
Cr_2O_3	0·04	0·04	0·03	n.a.	0·057	0·054	0·044	0·04	0·049	0·035	0·042	0·044	0·040	0·035
FeO*	10·19	9·75	11·52	10·91	9·69	10·05	9·82	9·46	10·48	10·61	11·35	10·99	10·49	11·02
MnO	0·23	0·29	0·25	0·15	0·15	0·17	0·24	0·21	0·17	0·13	0·16	0·18	0·13	0·15
MgO	8·40	8·41	7·08	7·88	8·42	8·18	8·29	8·35	8·35	7·84	7·82	7·96	8·48	8·28
NiO	0·02	0·02	0·02	n.a.	0·018	0·020	0·018	0·02	0·017	0·015	0·010	0·015	0·020	0·018
CaO	12·97	13·24	12·45	12·96	13·15	13·49	13·21	12·88	12·97	12·78	13·17	13·08	12·72	13·15
Na_2O	2·10	2·03	2·36	2·19	1·90	1·88	2·05	2·02	2·00	2·05	2·09	2·11	2·07	2·17
K_2O	0·07	0·06	0·18	0·18	0·11	0·12	0·10	0·15	0·16	0·19	0·24	0·17	0·16	0·25
P_2O_5	n.a.	n.a.	0·10	n.a.	0·110	0·109	n.a.	n.a.	0·118	0·165	0·202	0·177	0·164	0·165
Sum	98·25	97·63	98·52	97·92	98·61	98·67	97·47	97·49	98·74	98·85	99·94	99·79	99·41	99·45
Corresponding bulk rocks														
SiO_2	44·51	44·11	44·87	44·35	43·88	43·58	45·11	45·24	45·08	44·67	45·00	44·26	45·42	44·18
TiO_2	1·01	0·84	1·18	0·99	0·90	0·86	1·00	0·97	1·17	1·30	1·27	1·10	1·14	1·25
Al_2O_3	10·64	9·93	14·55	10·60	10·23	9·54	10·74	10·25	11·23	10·38	10·99	10·42	10·40	10·65
Cr_2O_3	0·268	0·242	0·059	n.a.	n.a.	n.a.	0·236	0·243	0·195	n.a.	0·210	0·197	0·184	0·181
Fe_2O_3	0·08	2·87	4·92	3·00	2·22	2·47	2·55	2·84	3·63	3·37	3·60	3·44	2·36	4·46
FeO	10·70	7·71	5·78	7·98	8·58	8·49	8·70	7·76	7·62	8·08	8·21	8·13	8·98	7·20
MnO	0·18	0·17	0·17	0·21	0·17	0·17	0·19	0·16	0·17	0·22	0·18	0·17	0·17	0·18
MgO	19·28	20·71	7·19	19·65	20·41	18·37	19·12	19·41	18·48	18·81	17·22	19·53	19·84	18·70
NiO	0·113	0·120	0·019	n.a.	n.a.	n.a.	0·109	0·134	0·112	n.a.	0·087	0·106	0·108	0·090
CaO	9·37	8·35	14·27	9·61	8·72	8·65	10·35	9·58	9·59	9·85	10·01	8·77	8·66	9·93
Na_2O	1·13	1·23	1·75	1·21	1·22	1·21	1·25	1·10	1·30	1·45	1·20	1·68	1·38	1·26
K_2O	0·02	0·07	0·03	0·11	0·01	0·05	0·05	0·11	0·18	0·07	0·06	0·04	0·12	0·08
P_2O_5	0·06	0·06	0·09	n.a.	0·07	0·07	0·08	0·08	0·09	0·11	0·15	0·12	0·12	0·14
Vol.	2·83	3·56	5·23	1·08	3·40	6·09	0·90	2·05	1·44	1·47	1·65	1·96	1·18	2·42
Sum	100·19	99·97	100·11	98·79	99·81	99·55	100·38	99·93	100·29	99·78	99·84	99·92	100·06	100·72

Analyses in wt % oxides. Each glass analysis is an average of 3–8 microprobe analyses. FeO*, total iron as FeO. Values for Cr_2O_3, NiO and P_2O_5 with three decimal places are high-precision analyses (see text). Bulk rocks were analysed in GEUS's chemical laboratory, mainly by XRF; Na_2O by AAS and FeO by titration. Vol, volatiles, calculated as loss on ignition corrected for oxygen uptake during ignition; n.a., not analysed.

inclusions often have lower Fe contents than expected from bulk-rock compositions (Gurenko *et al.*, 1996). To arrive at original melt compositions the lost iron has to be calculated back in by a stepwise procedure (Gurenko *et al.*, 1996).

Figure 12 shows the results of the combined effects of olivine crystallization and diffusional re-equilibration on the composition of the glass inclusions. As a result of re-equilibration, the Fe contents in the glass inclusions and the host olivines are strongly positively correlated, whereas the increased SiO_2 in the inclusions relative to the matrix glasses is a result of crystallization of olivine on the inclusion walls. The glass inclusions in the most Mg-rich olivines tend to have the highest SiO_2 contents and thus to have crystallized most olivine, which is explicable because these inclusions have been entrapped through the largest temperature interval before quenching.

The contents of MgO in the glass inclusions are not dependent on the composition of the host olivines (Fig.

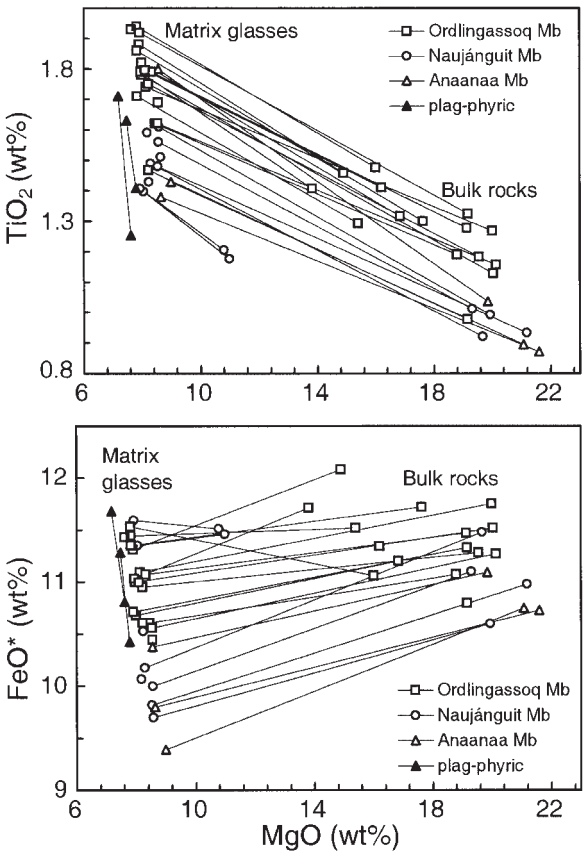

Fig. 11. Composition of matrix glasses (microprobe analyses) and corresponding bulk rocks of the Vaigat Formation. Lines connect the glasses to the corresponding bulk-rock compositions. The lines are subparallel because glasses with high TiO_2 and high FeO* come from bulk rocks with high TiO_2 and high FeO*, reflecting initial differences in the parental melts. In particular, the Ordlingassoq Member rocks and glasses have high TiO_2 and FeO*. There is thus not one combined liquid line of descent but a whole series of individual, parallel liquid lines of descent at different levels of TiO_2 and FeO*. The liquid lines of descent are approximated by the tie-lines in the TiO_2–MgO diagram because TiO_2 is incompatible during olivine fractionation. Two plagioclase-phyric basalts have different tie-line directions. (See text for discussion.)

12). Rather, the smaller inclusions have lost most MgO and the larger inclusions (>50 μm) the least. The small inclusions also tend to have the highest SiO_2 but some large ones also have high SiO_2.

Figure 13 shows clearly that there is no magmatic equilibrium between most of the inclusion glasses and their host olivines. Equilibrium requires an olivine–liquid FeO–MgO distribution coefficient (K_D) close to 0·3 (Roeder & Emslie, 1970; Ulmer, 1989), and oxidation of 15% of the Fe in the glasses (see later) brings only the matrix glasses and a few inclusion glasses down to the equilibrium K_D line. It is necessary to oxidize up to 60% of the iron in some of the glass inclusions to bring them all down to the equilibrium line, and this is not realistic for magmatic conditions.

CRYSTALLIZATION CONDITIONS FOR THE MATRIX GLASSES

Whereas the composition and P–T relations for the parental melts may be subject to discussion, the end points of crystallization, represented by the glassy rocks (~70 vol. % glass), are fairly certain. The melts were quenched close to 1 atm pressure to glasses in equilibrium with olivine and chromite, and the quench temperatures and oxygen fugacities can be calculated.

Glass quench temperatures

Quench temperatures can be calculated from equilibrium pairs of matrix glass and olivine rims bordering the glass, if the oxidation state of the melt is known or inferred. For reasons given below we used atomic $Fe^{3+}/\Sigma Fe$ = 0·15 for the glasses. Ford *et al.* (1983) provided an olivine–liquid thermometer together with a useful method for calculating a theoretical equilibrium olivine and the temperature (T_{sum}) for any given melt composition. We used this method for calculating the temperatures of all the analysed matrix glasses because in many samples the necessary olivine rims were not analysed. As shown in Fig. 14, quench temperatures are in the range 1180–1210°C for the olivine-phyric glasses and 1160–1180°C for four plagioclase–olivine-phyric glasses. The calculated equilibrium olivines have *mg*-number 81·5–86·5 for the olivine-phyric glasses and *mg*-number 78·3–81·9 for the plagioclase–olivine-phyric glasses. In samples where calculated and measured olivines can be compared, they are concordant within less than one *mg*-number.

Glass oxidation states

Matrix glass–spinel equilibrium pairs provide independent estimates of the oxidation state of the quenched melts. Maurel & Maurel (1982) found for 1 atm experiments at T = 1180–1300°C and fO_2 = 10^{-9}–10^{-3} a simple relation between Fe^{2+}/Fe^{3+} in spinel and coexisting melt:

$$\log_{10}(Fe^{2+}/Fe^{3+})_{sp} = 0{\cdot}764 \log_{10}(Fe^{2+}/Fe^{3+})_{liq} - 0{\cdot}343.$$

Application of this relation to 12 matrix glass–chromite pairs in assumed equilibrium resulted in calculated atomic $Fe^{3+}/\Sigma Fe$ for the glasses of 0·10–0·23. Eight glasses have $Fe^{3+}/\Sigma Fe$ = 0·16–0·18, and the coexisting chromites have $Fe^{3+}/\Sigma Fe$ = 0·38–0·41. The relatively high degree of oxidation is confirmed by Mössbauer analysis of one

Table 4: Glass inclusions in olivines from the Vaigat Formation

	1	2	3	4	5	6	7	8
Sample:	400452	332771	362148	136943	400452	136943	332771	362148
SiO_2	51·09	54·25	51·28	52·00	54·96	51·58	51·51	50·84
TiO_2	1·59	1·00	1·86	1·39	0·83	2·74	1·27	1·30
Al_2O_3	16·91	15·23	17·56	13·89	17·42	17·26	14·92	17·14
Cr_2O_3	0·17	0·12	0·09	0·15	n.d.	0·22	0·11	0·80
FeO*	5·28	4·95	4·80	6·87	6·16	6·06	8·23	7·65
MnO	n.d.	n.d.	0·10	0·07	n.d.	n.d.	0·19	0·10
NiO	n.d.	0·22	0·11	0·07	n.d.	n.d.	0·14	n.d.
MgO	6·87	8·66	4·53	8·15	4·21	2·99	7·69	4·02
CaO	15·13	12·65	15·21	13·51	13·24	12·93	12·80	14·67
Na_2O	2·02	2·39	2·60	2·33	3·10	3·63	2·30	2·62
K_2O	0·12	0·08	0·12	0·17	n.d.	0·35	0·14	0·11
Sum	99·20	99·56	98·26	98·60	99·96	97·78	99·30	99·26
Size (μm)	20	50	30 × 40	70	8	40	45	30
Ol. *mg*-no.	92·80	92·07	91·63	90·04	88·44	88·34	87·71	86·63

Analyses in wt % oxides. Most analyses are averages of 2–3 microprobed spots. *mg*-number is atomic 100 Mg/(Mg + Fe); *mg*-number in the enclosing olivine was measured in the same analytical run (see text). n.d., not detected. Petrographic notes: 1 and 5 are enclosed in the same olivine crystal. 4, Inclusion in the crystal shown in Fig. 3a. 6, inclusion in speckled olivine core (Fig. 3g). The glass is heterogeneous.

of the 12 glasses (264137, Table 3), which gave $Fe^{3+}/\Sigma Fe_{(glass)} = 0{\cdot}18$, where the Maurel & Maurel (1982) algorithm for the same sample gave $Fe^{3+}/\Sigma Fe_{(glass)} = 0{\cdot}16$. The lower and higher degrees of oxidation calculated for some samples are possibly real but can also be due to lack of equilibrium between the analysed phases.

Given the temperatures and the oxidation states of the quenched glasses, the oxygen fugacities can be calculated following Kilinc *et al.* (1983). The resulting fO_2 values are in the range $10^{-6{\cdot}3}$–$10^{-7{\cdot}1}$, which around 1180–1200°C corresponds to around one $\log_{10}$ unit above the nickel–nickel oxide (NNO) buffer and 1·5–2 $\log_{10}$ units above the fayalite–magnetite–quartz (FMQ) buffer. Comparison of the chromites with the experimental spinels of Murck & Campbell (1986) and Balhaus *et al.* (1991) similarly suggests that spinels with $Fe^{3+}/\Sigma Fe$ around 0·4 at 1200°C formed above the NNO buffer. The experiments of Balhaus *et al.* were performed at high pressures, but the $Fe^{3+}/\Sigma Fe$ ratios of the spinels are primarily dependent on the oxidation state of the melts and are only very slightly pressure dependent.

Christie *et al.* (1986) found that MORB pillow glasses have oxidation states around two $\log_{10}$ units below the NNO buffer, corresponding to $Fe^{3+}/\Sigma Fe$ around 0·07, and that the crystalline pillow interiors are more oxidized with $Fe^{3+}/\Sigma Fe$ around 0·19, 1–1·5 $\log_{10}$ units higher than the glasses but still below the NNO buffer. They suggested that the crystalline parts are oxidized as a result of hydrogen loss during crystallization.

The relatively high oxidation states of the Vaigat Formation glasses could perhaps be explained by the fact that most of the pillow breccias were formed after the subaerial lavas flowed into water so that they may have been degassed and oxidized before quenching. However, chromites enclosed in pre-eruption olivine phenocrysts with *mg*-number >89 have only slightly lower $Fe^{3+}/\Sigma Fe$ than those in equilibrium with the glasses (Table 2). They show some variation in oxidation state ($Fe^{3+}/\Sigma Fe = 0{\cdot}23$–$0{\cdot}48$) but still correspond to redox conditions close to the NNO buffer. Thus, in accordance with Pedersen (1985), we suggest that the Vaigat Formation magmas were inherently more oxidized than MORB magmas and crystallized close to and above the NNO buffer. In the olivine–liquid calculations we have consequently used a value of $Fe^{3+}/\Sigma Fe$ of 0·15 for the matrix glasses, which is a minimum estimate but facilitates the comparison with other datasets where this value is commonly used, for example, that of Albarède (1992). Similarly, Francis (1985) noted that in the Baffin Island picrites 15% iron in oxidized form is required for equilibrium between glass and olivine rims. Indeed, we can in several cases improve the match between measured and calculated olivine by oxidizing up to 20% of the iron in the glass.

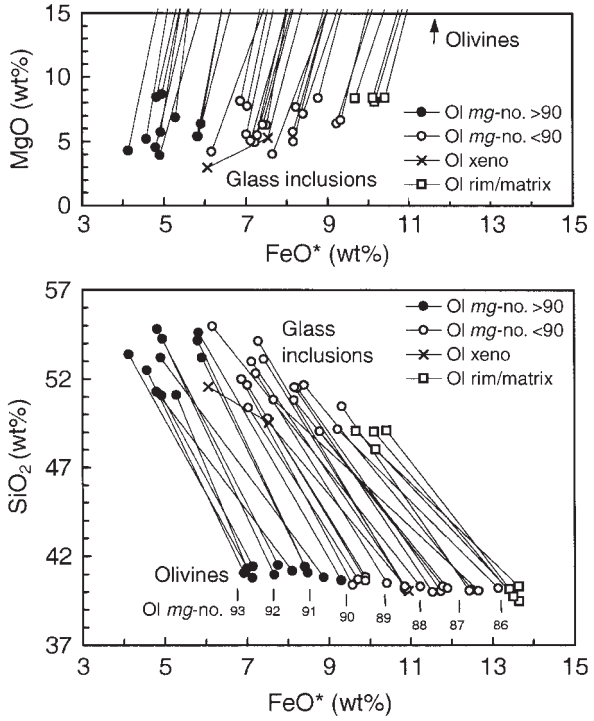

Fig. 12. Composition of glass inclusions in olivines (microprobe analyses of unheated inclusions). Lines connect the inclusions with the enclosing olivines (off-scale in upper diagram). Matrix glasses and coexisting groundmass olivine rims are included for comparison (□, from the same samples as the glass inclusions). (Note the general trend of decreasing FeO* and increasing SiO_2 for inclusions in increasingly magnesian olivines, whereas the MgO contents vary more irregularly.) In both diagrams the Mg-rich olivines and their inclusions are end members of smooth series, indicating that all are comagmatic. (See text for discussion.)

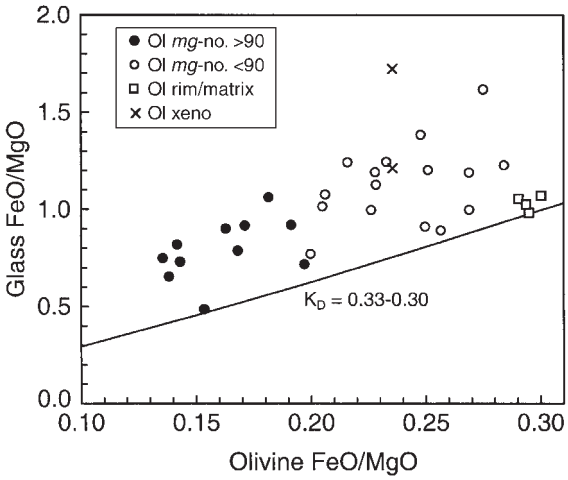

Fig. 13. FeO/MgO in glass inclusions vs FeO/MgO in the enclosing olivines. Matrix glasses and coexisting groundmass olivine rims are included for comparison (□). FeO in the glass analyses was calculated assuming 15% of the iron in oxidized form. For equilibrium, the points should lie close to the K_D line. K_D is considered to be pressure dependent (Ulmer, 1989), and therefore the K_D line shown was calculated with K_D varying from 0·33 in the left (high-pressure) side to 0·30 in the right (low-pressure) side of the diagram. It should be noted that matrix glasses and coexisting olivine rims are close to equilibrium but most other olivines and glass inclusions are not. To shift all points down to the equilibrium line it is necessary to assume that up to 60% of the iron in the inclusions is Fe^{3+}, and >20% Fe^{3+} is not realistic for magmatic conditions. There is thus no magmatic equilibrium between most inclusions and their host olivines.

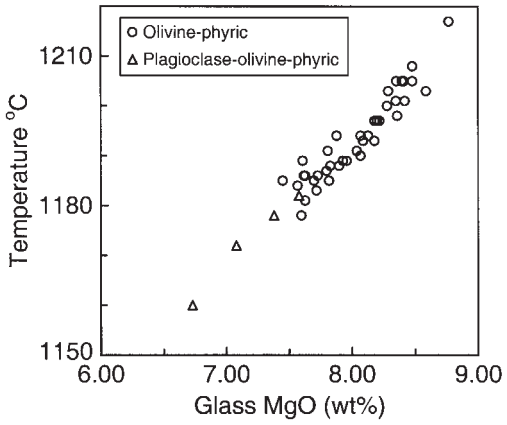

Fig. 14. Quench temperatures for all analysed matrix glasses from the Vaigat Formation, calculated after Ford *et al.* (1983), the T_{sum} method.

Mg-RICH HIGH-TEMPERATURE MELTS

Phenocryst–melt relations

The occurrence of olivine-rich picritic rocks does not necessarily prove that Mg-rich melts existed because the rocks may consist of relatively Mg-poor melt with accumulated olivine crystals. However, the highly magnesian olivines with high contents of Ca and Cr and with glass inclusions, precluding the possibility that they are mantle xenocrysts, indicate that highly magnesian parental melts did exist. For an olivine–liquid Fe–Mg K_D of 0·33 (see below), olivines with *mg*-number 92–93 are in equilibrium with melts with *mg*-number 79–81·5. The bulk rocks of the Vaigat Formation with *mg*-number 79–81 have 19–22 wt % MgO and could thus be representative of the parental melts, as concluded by Clarke (1970). However, the observed modal proportions of Mg-rich olivine in the rocks are far from the proportions expected for such melts. The expected modal proportions of olivine in a melt can be calculated by simple stepwise subtraction of equilibrium olivine. Such calculations show that a melt with a composition like a typical bulk rock with ~20 wt % MgO will by fractional crystallization precipitate >10 vol. % olivine with *mg*-number >90. In strong contrast, such olivines constitute <1 vol. % of the actual rocks. The majority of the olivine phenocrysts in the rocks have compositions of *mg*-number 86–89 (Fig. 4), which would be in equilibrium with melts with 10–14

wt % MgO. There are two possible explanations for this (which are not mutually exclusive). Either, the ultramafic parental melts fractionated olivine with *mg*-number 93–86 at depth until there was 14–10 wt % MgO in the melts; most of the early-formed high-Mg olivines were left at depth, and the melts erupted charged with accumulated later-formed olivine with *mg*-number 89–86, bringing many of the bulk compositions back to as high MgO contents as those of the parental melts and sometimes higher (Fig. 1). Alternatively, the parental melts underwent closer to equilibrium crystallization at depth, with the earlier formed olivines being re-equilibrated by diffusion to successively more iron-rich compositions. The second explanation was favoured by Francis (1985), who concluded that the bulk rocks therefore can be considered representative of the original melts, and the Mg-rich olivines are xenocrysts. Our data show, however, that the Mg-rich olivines are integral parts of the cognate mineral assemblage of the West Greenland picrites (Figs 5, 7 and 12). Further, the olivine and chromite phenocrysts are to a large extent not re-equilibrated. The olivines are strongly zoned, and crystals with individually different compositions are preserved (Fig. 7).

The zoning profiles of the olivine phenocrysts shown in Fig. 6 provide clues to crystallization mechanisms. The smoothly curved profile in Fig. 6c, with steepening gradients towards the rims, closely matches the theoretical profile calculated for simple fractional crystallization. The very magnesian cores with *mg*-number >92 in Fig. 6a and b are virtually unzoned, suggesting crystallization closer to equilibrium conditions. The sharp slope breaks between cores and rims in these two crystals indicate change of mechanism. Sharp slope breaks and flat profile centres may also be seen in acentral crystal sections (Pearce, 1984), but this would mean that the true centres must have even higher *mg*-numbers, which is improbable. The two olivine crystals shown in Fig. 6a and d, from the same sample, have near-linear marginal zoning profiles. This can be produced either by an accelerating crystallization rate that fortuitously leads to linear profiles, or, more probably, by re-equilibration by diffusional exchange between olivine and liquid, as shown by Maaløe & Hansen (1982). The centre of the smaller crystal (as cut by the section) is modified throughout. The thin rims on the *mg*-number 92·5 core in Fig. 6b are probably produced by growth of new olivine during and after entrainment and eruption.

Maaløe & Hansen (1982) and Maaløe *et al.* (1989) described olivine zoning profiles in Hawaiian basalts very similar to those in Fig. 6b and c, and they concluded that the olivines formed under supercooled conditions and variable growth rates during successive stages of evolution of the melts. They did not find rims with linear zoning profiles like those in Fig. 6a and d, and they concluded that diffusional re-equilibration was minimal. The West Greenland data indicate that the olivines in some samples did partly re-equilibrate (e.g. 362148): the crystal shown in Fig. 6a consists in plane section, as revealed by scanning electron micrographs, of nearly equal areas of homogeneous core and re-equilibrated rims, and in three dimensions thus more than three-quarters of the original crystal is re-equilibrated. In rare samples (four found among 56 microprobed) the olivines equilibrated completely with the liquid (e.g. 264217, right panel in Fig. 7). In most cases, however, re-equilibration was minimal, and this process cannot account for the lack of olivine with *mg*-number >90. We must conclude that a large amount of high-Mg olivine fractionated out and was left behind in the conduit systems at depth during the magma's ascent towards the surface.

Composition and temperature of the parental melts

The loss of most of the high-Mg olivines (*mg*-number >90) and the accumulation of more iron-rich olivines (*mg*-number <90) in the conduit systems during magma ascent show that the bulk rocks do not directly represent the parental melt compositions. By parental melts we understand the most primitive melts recorded in the mineral compositions; however, because the olivines go up to *mg*-number >92 these may be in equilibrium with mantle olivine and the parental melts may be close to also being primary mantle melts.

Because olivine and chromite are the only fractionating phases the compositions of the parental magnesian melts may be calculated by starting from the matrix glasses and adding equilibrium olivine back in successive steps until the equilibrium olivine has the same composition as the most magnesian olivine in a sample. This is a standard method used by many workers, e.g. Albarède (1992) and Sobolev & Nikogosian (1994). Results of such calculations for the Vaigat Formation are shown in Tables 5 and 6. The results are dependent on assumptions with regard to the most magnesian olivine, the oxidation state of the melts, and the pressure increase with depth. The most magnesian olivine was defined as *mg*-number 92·5 for all samples from the Anaanaa and Naujánguit Members, and *mg*-number 92·0 for all samples from the Ordlingassoq Member, because these values are the normal maximum values for the olivines in the respective formations. The minor elements Cr and Ni in the added olivine were adjusted in steps in accordance with the measured concentrations. In the matrix glasses, 15% of the iron was oxidized in accordance with the measured oxidation states; this corresponds to fO_2 values one log-unit above the NNO buffer (NNO + 1). No further adjustments of the oxidation state were made, which means that fO_2 decreased during olivine addition to close

to and slightly above the NNO level at the end of calculations. Another possibility is to adjust the oxidation stage to a buffer curve, and this has pronounced effects on the results (Table 6), but there is no geological reason why the melt's fO_2 path should be parallel to the synthetic curves. The pressure increase with depth, required for the calculation of olivine K_D values (Ulmer, 1989), was assumed to be linear at 0·2 kbar per 0·5 wt % olivine added because this ends the procedure at depths in the uppermost lithospheric mantle (13–16 kbar), but other choices are possible (Table 6). Equilibrium with olivine *mg*-number 92·0 or 92·5 was obtained when the calculated melts consisted of 28–34 wt % olivine and 66–72 wt % glass. Figure 15 illustrates that the composition of a calculated melt is rather sensitive to the composition of the olivine at which the procedure is stopped, and Table 6 illustrates the effects of varying fO_2 and pressure in the calculations for one sample. However, the differences between the samples calculated with one set of assumptions are maintained when the assumptions are changed.

The calculated parental melts (Table 5) contain 20–21 wt % MgO, similar to or slightly higher than the bulk rocks. The differences are also small for elements that are incompatible during olivine fractionation, and all ratios of such elements (e.g. CaO/Al_2O_3) are preserved. The major difference between the calculated melts and the bulk rocks lies in FeO*, this being 0·5–1 wt % lower in the calculated liquids than in the bulk rocks. As shown by three examples in Fig. 16, this is because the equilibrium olivines added in the calculations become successively more Fe poor, and in liquids with more than ~13 wt % MgO the added olivines (*mg*-number >88·5) contain less iron than the liquid. These Mg-rich, Fe-poor olivines constitute a major part of the olivine assemblage in the calculated liquids, whereas the olivines in the bulk rocks are more Fe rich, with a frequency peak at *mg*-number 86–88·5 (Fig. 4).

The content of Cr_2O_3 in the parental melt was estimated from Cr_{ol}–Cr_{liq} partitioning because the modal amounts of chromite involved, which completely dominate the Cr inventory, are unconstrained. The most Mg-rich olivines contain ~0·15 wt % Cr_2O_3, and a partition coefficient Cr_{ol}–Cr_{liq} of 0·5 (Hanson & Jones, 1998) thus gives 0·30 wt % Cr_2O_3 in the parental melt. Therefore, 0·6 wt % chromite was added to the calculated parental melt to increase the Cr_2O_3 content to 0·30 wt %. This value is distinctly higher than that of the bulk rocks with 20–21 wt % MgO, which have on average 0·22 ± 0·03 wt % Cr_2O_3 (Table 3 and unpublished data, 2000). The result suggests that more chromite has been lost by fractionation than has been acquired by accumulation—which is geologically reasonable.

The content of NiO in the parental melt should be higher than in the bulk rocks because the bulk rocks contain less magnesian olivines with less NiO than the melts would have done. The difference is, however, only ~0·02 wt % as estimated from the measured contents of NiO in the olivines. Accordingly, the calculated parental melts have 0·12 wt % NiO (Table 5), whereas the bulk rocks with 20–21 wt % MgO have on average 0·11 ± 0·01 wt % NiO (Table 3 and unpublished data, 2000). The NiO contents in the bulk rocks thus approximate those of the parental melts fairly well. With 0·46 wt % NiO in olivine *mg*-number 92 and 0·12 wt % NiO in the parental melt, olivine–liquid partition coefficients for Ni close to four are indicated. This is less than found in the experiments by Hart & Davis (1978), but similar to other high-temperature results summarized by Elthon & Ridley (1979).

The calculated temperatures for the parental melts are very high, 1500–1560°C. These results are supported by the composition of the Mg-rich olivines and chromites. Olivines as Cr rich as those in the Vaigat Formation are found only in komatiites and other ultramafic igneous rocks equilibrated at high temperatures, in accordance with the experimental data of Li *et al.* (1995) that suggest 1 atm temperatures of ~1450°C for olivines with 0·1 wt % Cr_2O_3 at FMQ. Similarly, the 1 atm experiments on the Kambalda komatiite by Murck & Campbell (1986) produced olivine–chromite pairs similar to the high-Mg mineral pairs in the Vaigat Formation only at 1400°C or higher temperatures. Attempts to simulate crystallization of the measured olivine–chromite pairs from the calculated parental melts with the program SPINMELT (Ariskin & Nikolaev, 1996) resulted in temperatures of 1450–1570°C, but the calculated spinel compositions were variable and extremely dependent on small variations in the estimated Cr contents in the melts and the assumed pressures.

Mantle melting conditions

The West Greenland lavas were produced beneath a rifting continent. Holm *et al.* (1993) showed that the melts were produced in the asthenospheric mantle and found Sr and Nd isotopic differences between the Naujánguit and Ordlingassoq Members indicating more of a depleted MORB-type component in the Naujánguit Member and more of an Iceland-plume-type component in the Ordlingassoq Member. The calculated parental melts in Table 5 show compositional differences between the Anaanaa and Naujánguit Members on one hand and the Ordlingassoq Member on the other hand, with Ordlingassoq Member having higher FeO* and TiO_2. These differences are present in the matrix glasses as well as in the bulk-rock analyses (Fig. 11) and must have arisen during mantle melting. Because the isotopes indicate variable amounts of different mantle components,

Table 5: Calculated compositions of parental melts in the Vaigat Formation

	Anaanaa Mb	Naujánguit Mb		Ordlingassoq Mb		
Sample:	400452	332771	362148	136943	156737	264105
SiO_2	46·63	46·63	46·88	45·71	46·35	45·77
TiO_2	0·99	1·08	1·15	1·13	1·30	1·18
Al_2O_3	10·12	9·88	10·54	10·76	9·72	9·70
Cr_2O_3	0·30	0·30	0·30	0·31	0·30	0·30
Fe_2O_3	1·22	1·22	1·21	1·26	1·26	1·26
FeO	8·81	8·89	8·60	9·40	9·53	9·72
MnO	0·27	0·23	0·21	0·18	0·15	0·19
MgO	20·42	20·61	19·83	20·30	20·85	21·40
NiO	0·14	0·11	0·13	0·13	0·14	0·15
CaO	9·55	9·45	9·49	9·22	8·77	8·72
Na_2O	1·45	1·45	1·47	1·41	1·39	1·39
K_2O	0·04	0·07	0·11	0·11	0·13	0·11
P_2O_5	0·07	0·07	0·07	0·08	0·11	0·11
Sum	100·00	100·00	100·00	100·00	100·00	100·00
Melt *mg*-no.	80·51	80·51	80·42	79·37	79·58	79·69
FeO*	9·90	9·98	9·69	10·53	10·66	10·86
% iron ox.[a]	11·06	10·95	11·21	10·75	10·60	10·45
CaO/Al_2O_3	0·94	0·96	0·90	0·86	0·90	0·90
wt % minerals added						
Olivine	29·6	30·3	28·2	30·0	32·4	33·7
Chromite	0·6	0·6	0·6	0·6	0·6	0·6
Equilibrium olivine						
mg-no.	92·48	92·46	92·48	91·97	91·98	91·98
Olivine K_D[b]	0·336	0·337	0·334	0·336	0·340	0·342
Temperatures and pressures of parental melts						
T (°C)[c]	1528	1534	1515	1528	1544	1559
P (kbar)[d]	14·0	14·4	13·2	14·2	15·6	16·4
Temperatures and pressures of primary melt segregation						
Alb. 92, *T*(°C)	1578	1582	1563	1584	1590	1606
Alb. 92, *P* (kbar)	30·2	30·5	28·2	34·2	32·2	36·0
Max *mg*-no. meas. in olivine	92·86	92·38	93·10	92·24	91·30	91·60

Melts calculated by addition of equilibrium olivine in 0·5% steps to the matrix glasses in Table 3. (For details of calculation method, see text.)
[a]No adjustments to fO_2 during olivine addition.
[b]Olivine K_D formulation from Ulmer [1989, equation (13)].
[c]From Ford *et al.* (1983, T_{sum}).
[d]Model-dependent: assuming a pressure increase of 0·2 kbar per 0·5% olivine added.
Alb. 92: Albarède [1992, equations (2) and (3)].

whereas the calculated temperatures for all members are similar (Table 5), we suggest that the main cause for the differences in parental melt composition lies in different mantle source compositions whereas the melting processes were similar.

The parental melts calculated here have FeO* contents that are lower than those in the bulk rocks by 0·5–1·0 wt %. This is significant for the estimation of the depth of melting (e.g. Elliott *et al.*, 1991). In melting models such as that of Langmuir *et al.* (1992) it would correspond

Table 6: Calculated melts in the Vaigat Formation in equilibrium with olivine mg*-number 92·5: dependence of results on* fO_2 *and pressure for one sample (GGU 362148)*

	d*P*/dxol[a]	*T* (°C)[b]	*P* (kbar)	MgO	FeO*	% Fe ox[d]	% ol added[e]
log fO_2							
NNO + 1	0·0	1401	0	17·4	9·7	13·5	22·2
Variable[c]	0·0	1407	0	17·7	9·7	11·6	23·0
NNO	0·0	1423	0	18·5	9·7	8·6	24·9
FMQ	0·0	1435	0	19·0	9·7	5·9	26·7
NNO + 1	0·1	1435	5·3	17·9	9·7	15	23·3
Variable[c]	0·1	1455	5·8	18·7	9·7	11·2	25·2
NNO	0·1	1470	6·3	19·4	9·7	9·2	27·1
FMQ	0·1	1480	6·6	19·8	9·7	7·1	28·2
NNO + 1	0·2	1482	11·6	18·6	9·7	15	25·2
Variable[c]	**0·2**	**1515**	**13·2**	**19·8**	**9·7**	**11·2**	**28·2**
NNO	0·2	1525	13·8	20·2	9·7	9·8	29·2
FMQ	0·2	1536	14·4	20·7	9·7	8·9	30·3
NNO + 1	0·3	1537	19·2	19·6	9·6	16·1	27·4
Variable[c]	0·3	1586	22·5	21·2	9·6	10·4	31·3
NNO	0·3	1594	23·1	21·4	9·7	10·8	32·0
FMQ	0·3	1596	23·4	21·5	9·7	11·2	32·4

[a]Pressure increase, kbar per 0·5% olivine added.
[b]From Ford *et al.* (1983, T_{sum}).
[c]Olivine added with no adjustment of the Fe oxidation ratio to a buffer curve: start points in glass at NNO + 1 and end points close to the NNO buffer. fO_2 values calculated after Kilinc *et al.* (1983). Buffer curves from Frost (1991).
[d]Percentage of iron in oxidized form.
[e]Wt % of olivine added to the matrix glass.
The model in bold type is used in Table 5.

to a pressure decrease of 5–10 kbar. Holm *et al.* (1993) suggested that a bulk-rock data trend extending to high levels of FeO* at constant Al_2O_3/TiO_2 is a consequence of deep melting of the hot mantle plume source. However, we consider that it is solely a consequence of iron-rich olivine accumulation.

Segregation pressures for the primary melts have been estimated by Clarke (1970), Herzberg (1995) and Herzberg & Zhang (1996) at 30–40 kbar, based on bulk-rock CaO/Al_2O_3, and this result is still valid because CaO/Al_2O_3 is insensitive to compositional and modal variations in the olivines. Herzberg & O'Hara (1998) estimated average segregation pressures for the West Greenland picrites of ~38 kbar and initial melting pressures of ~45 kbar, and these estimates are also valid because the calculated parental liquids in Table 5 plot similarly to the bulk rocks with 20–21 wt % MgO in the CMAS projections used. The segregation pressures calculated with the simple algorithms of Albarède (1992) are 28–36 kbar, that is, somewhat lower in comparison.

Segregation temperatures calculated for the parental melts after Albarède (1992) are 1563–1606°C (Table 5). For the relevant pressures, this corresponds to mantle potential temperatures of 1520–1550°C, in excellent agreement with the estimates by Gill *et al.* (1992) and Herzberg & O'Hara (1998). The ~50°C difference between the temperatures calculated at segregation depths and in the upper lithospheric mantle is an effect, partly of the pressure differences and partly of the latent heat of fusion.

PROCESSES IN THE CONDUIT SYSTEMS

If the final pressures of segregation were ~30 kbar the melts segregated at ~140–100 km depth, indicating the existence of a lithospheric lid of ~100 km thickness that curtailed the melting column. The melts thus ascended through roughly 100 km of conduit systems in the lithospheric mantle and crust. The depth interval of the conduit systems for which evidence of crystallization is preserved in the erupted lavas is unconstrained. We have put the deepest part at pressures of 13–16 kbar (Table

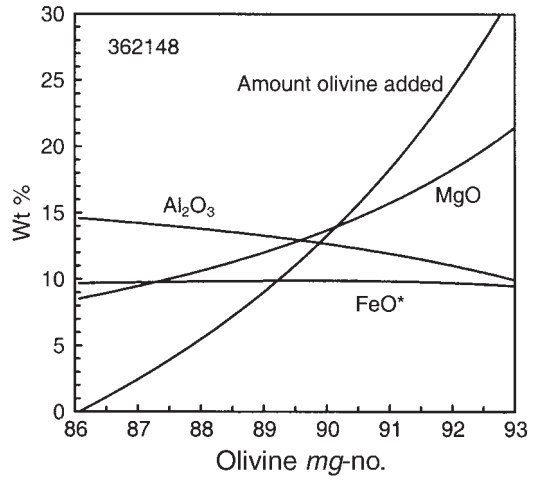

Fig. 15. Development in composition of the calculated melt during addition of equilibrium olivine, starting from the matrix glass composition, exemplified for sample GGU 362148. (See text for details of calculation.) The composition of the parental melt is fairly sensitive to the composition of the olivine at which the procedure is stopped. The parental melt listed in Table 5 was calculated up to olivine *mg*-number 92·5 and has 19·83 wt % MgO, 10·54 wt % Al_2O_3 and 9·69 wt % FeO*; if the calculation is stopped at olivine *mg*-number 92·0, the parental melt will have 18·28 wt % MgO, 11·08 wt % Al_2O_3 and 9·80 wt % FeO*. The sensitivity of the MgO content increases at high olivine *mg*-number.

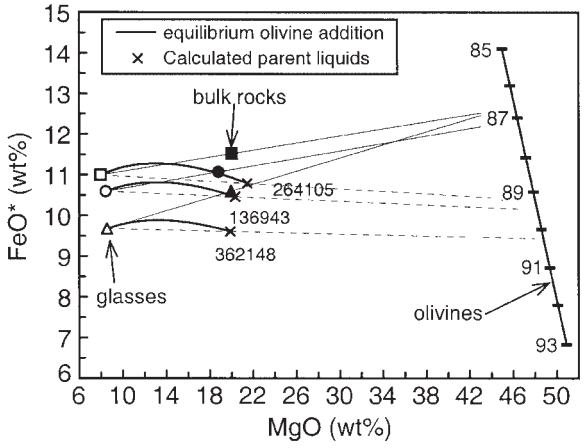

Fig. 16. FeO* vs MgO for matrix glasses (open symbols), corresponding bulk rocks (closed symbols), and calculated parent liquids (crosses), for three samples spanning a range of iron contents. The curved lines are trajectories followed by stepwise addition of equilibrium olivine to the glasses. The calculated parent liquids are in equilibrium with olivine *mg*-number 92·0 (136943 and 264105) or *mg*-number 92·5 (362148). Thin dotted lines connect glasses and corresponding parent liquids and project towards olivine compositions around *mg*-number 89–90·3, the average olivine added to the glass. Thin continuous lines connect glasses and corresponding bulk rocks and project towards olivine compositions around *mg*-number 87, the average olivine in a sample. The bulk rocks have lost Mg-rich olivines and accumulated more iron-rich olivines relative to the parent liquids.

5), i.e. in the uppermost lithospheric mantle. Considering the shallower parts, the fractionated melts always crystallized plagioclase before clinopyroxene, as evidenced by the plagioclase-phyric basalts and rare small cognate xenoliths of troctolitic gabbros. Modelling with the computer program COMAGMAT (Ariskin *et al.*, 1993) indicates that the two-phase cotectic was reached at pressures of 3 kbar or lower because at higher pressures clinopyroxene would crystallize before plagioclase. Thus, the vertical extent of the zone of major crystallization is estimated to be situated at depths from 40–50 km to <9 km, and in principle it reached to the surface.

The scarcity of picrites in most flood basalt successions has been ascribed to density trapping of the primary Mg-rich melts in sill-like complexes at the crust–mantle boundary where the olivines are deposited in ultramafic cumulates, and only the evolved basaltic melts are erupted (Cox, 1980). The eruption of picrites requires that a density trap does not exist or is circumvented, and the conduits are most likely to be steep and dyke like. In West Greenland, the conduits were also very crystal rich, and the preserved olivines and chromites provide evidence for complex open-system processes of equilibrium and fractional crystallization, magma mixing, oxidation, and partial to complete re-equilibration. We envisage that crystal-charged magma batches ascended through irregular, dyke-like conduits, precipitating high-Mg olivines (*mg*-number 90–93) and chromites (*mg*-number 69–77) at deeper levels and less magnesian olivines (*mg*-number 86–88) and chromites (*mg*-number <69) at shallower levels. At high magma ascent rates many olivine crystals were kept in suspension all the way to the surface, even some of the deep high-Mg olivines, whereas at low ascent rates only few and small olivines were suspended and the magmas erupted as olivine-microphyric to aphyric basalts. Pulsating magma ascent would lead to mixing of magma batches in various stages of fractionation and equilibration. In stagnating magma pockets crystallisation proceeded to low-Mg olivines (*mg*-number 85–78) and rare troctolites later picked up in passing magmas. However, the majority of the magmas passed so fast that equilibration was far from complete, and their crystal assemblage consists of mechanical mixtures of crystals both from several magma batches and picked up from the sidewall at all depths. The significant variability of the contents of the minor elements Ca, Cr and Ni in olivine crystals in some samples (Fig. 7) can be explained as an effect of fractionation and mixing of magma batches. This process introduces variabilities that are directly proportional to the bulk distribution coefficients (Albarède *et al.*, 1997), and the variabilities should thus decrease in the order Cr (bulk $D \sim 6$) – Ni (bulk $D = 4$) – Ca (bulk $D = 0{\cdot}028$). This is in accordance with the observed variabilities in non-equilibrated samples (Fig. 7). Excess enrichment of incompatible elements in

the melt need not be detectable because the magmas did not go through many cycles and a steady state was not attained, as indicated by the large spread in MgO content of the erupted magmas down to 6·5 wt % MgO (Fig. 1). It is clear, however, that the back-calculation with stepwise addition of equilibrium olivine to the matrix glass (Table 5) is a simplification that works best for elements with partition coefficients around one.

The magma ascent velocity can be estimated in one case. The olivine crystal shown in Fig. 6a has rims of 0·4 mm width with linear zoning profiles, which we ascribe to diffusional re-equilibration with the melt (Maaløe & Hansen, 1982). The diffusion data of Jurewich & Watson (1988) indicate that rims of this width at 1300°C would have formed in a period of ~2 months. If the crystal formed in the deep part of the conduit system around, say, 30 km depth, this corresponds to a magma ascent velocity of 500 m/day, i.e. 0·6 cm/s. In comparison, Maaløe (1973) calculated ascent velocities of 1–10 cm/s for Hawaiian lavas carrying 2–20 cm olivine nodules. Considering that the olivines in the West Greenland picrites are normally not larger than 0·5 cm, the lower ascent velocity of 0·6 cm/s is in accordance with the Hawaii data.

Even the rare magma batches that erupted with completely re-equilibrated olivines apparently passed fast and without complete equilibration through the greater part of the conduits because their olivine assemblage is petrographically just as diverse as in the other rocks. The complete equilibration to olivine *mg*-number ~86·5 must have taken place in high-level ephemeral magma chambers where the melts evolved to MgO contents around 10 wt % at ~1250°C. The few plagioclase-phyric basalts would have developed in similar magma chambers.

The crystal-rich conduit systems envisaged here are sketched in Fig. 17. They have many features in common with the crystal-dominated 'slim-line' magma chambers proposed by Sinton & Detrick (1992) for mid-ocean ridges. These magma chambers are vertically extensive and consist of a central crystal-rich zone within which the magma can move, surrounded by a rigid, largely crystalline (>60% crystals) transition zone to the wall rocks. Despite the very different tectonic setting and lithosphere thickness of West Greenland, the magma conduits were apparently similar. The rifting continent may be viewed as a slow-spreading ridge environment with high magma supply rates, where the large magma volumes contributed less to lateral crustal accretion than they would do in an oceanic setting, and mainly formed new crust by aggradation at the surface. Features seen in West Greenland and noted by Sinton & Detrick (1992) as characteristic of slow-spreading ridges are the scarcity of evolved magmas, the frequency of mixed populations of crystals, and the association of magma conduits with

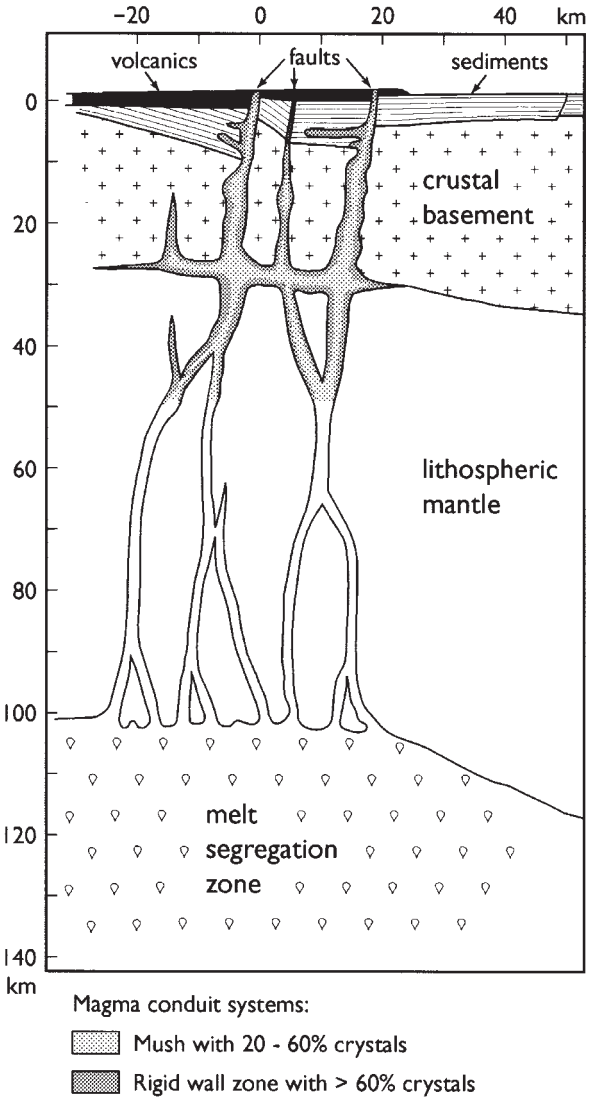

Fig. 17. Conceptual model of the conduit systems for the volcanic rocks of the Vaigat Formation in West Greenland. Asthenospheric mantle melts are segregated at 140–100 km depth and ascend through narrow dyke-like conduits in the lithospheric mantle and crust. Following the crystal-dominated magma chamber model of Sinton & Detrick (1992) the conduits are plated with a rigid zone that contains >60% olivine crystals and shields the interior zone from sidewall contamination. The interior zones through which the fractionating magma batches pass contain 20–60% crystals; the amount of crystals left behind in the conduits depends on the ascent velocity. We envisage that major crystallization started around 45 km depth and there was some modest magma accumulation at the crust–mantle boundary, but most magmas passed straight up. Passageways and eruption sites exploited fault-controlled zones (Pedersen *et al.*, 1996) but were not exclusively bound to these. Magma batches that intruded laterally into the crystalline basement or the sediments, of up to 8 km thickness, in the basin became contaminated and fractionated sulphides and occasionally native iron (Pedersen, 1979*b*, 1985; Lightfoot *et al.*, 1997). (Note very little crustal underplating.) Cross-section drawn after Chalmers *et al.* (1999).

syn-volcanic faults. However, there is no rift valley because of the high magma supply rate and the aggradation of the lava plateau. The vertical extent of the conduit system is much greater than at mid-ocean ridges because the lithosphere is much thicker. Sinton & Detrick (1992) noted that the MgO content of the cumulate crystals should increase with depth, similar to our interpretation for West Greenland. The applicability of similar magma chamber models to both oceanic spreading centres and a continental rift zone is supported by the work of Donaldson & Brown (1977), who described complex olivine populations very similar to those described here, but from MORBs. Despite the differences in lithosphere thickness, the processes in the conduit systems appear to be the same.

The conduit systems envisaged here for the Vaigat Formation would not have led to simple underplating but rather to an irregular vertical distribution of olivine cumulates across the mantle–crust boundary and throughout the crust, concentrated in zones of crustal extension (Fig. 17). Judged from the average MgO content of 15·5 wt % in the erupted lavas, on average 13 wt % of the parental melts was left behind as cumulate crystals in the conduit systems.

CONCLUSIONS

The uncontaminated picritic volcanic rocks of the Vaigat Formation contain 6·5–30 wt % MgO (average 15·5 wt %) and contain olivines with up to *mg*-number 93. The olivine crystals show zoning patterns indicating equilibrium and fractional crystallization, oxidation, partial and complete re-equilibration, and magma mixing. All the olivine crystals contain glass inclusions and have high contents of Ca and Cr, indicating that they precipitated from melts; even the most Mg-rich olivines are cognate phenocrysts. Mantle xenocrysts have not been found. The most Mg-rich rocks were erupted as melt–olivine mixtures. The erupted melts contained no more than up to 14 wt % MgO and were charged with olivine crystals with *mg*-number 78–93, most frequently *mg*-number 86–88·5, and associated chromites. The melts quenched in pillow breccias to glasses with ~8 wt % MgO at around 1200°C and $\log fO_2$ at NNO + 1, close to the olivine–plagioclase cotectic. The melts evolved along a number of individual liquid lines of descent; the differences were inherited from the primary melts and probably reflect compositional differences in the mantle sources.

The parental melts were not erupted. Their compositions were calculated by stepwise addition of equilibrium olivine to the matrix glasses; they had 20–21 wt % MgO at 1500–1560°C and fO_2 around NNO, and they are close to being primary magmas. Erupted rocks with around 20 wt % MgO as a result of accumulated olivine are similar to the parental melts in many respects, especially in incompatible and moderately compatible elements, but the rocks have higher FeO* contents than the melts by 0·5–1 wt % because most of the high-Mg olivines with *mg*-number 90–93 were lost in the conduit systems. Therefore, petrogenetic conclusions based on bulk-rock FeO* contents (Holm *et al.*, 1993) should be viewed with caution. Conclusions on melting depths based on CaO/Al_2O_3 and CMAS projections (Clarke, 1970; Herzberg, 1995; Herzberg & Zhang, 1996; Herzberg & O'Hara, 1998) are still valid.

The primary melts ascended in conduit systems of around 100 km vertical extent in the lithospheric mantle and crust, and no density traps such as sill-like magma pools at the crust–mantle boundary were in effect. Crystallization of olivine and chromite, preserved in the eruption products, took place from assumed depths of around 45 km and to the surface. The crystal-charged magmas precipitated high-Mg olivines and chromites at deep levels and less magnesian crystals at shallower levels. Rapidly ascending magma batches carried large amounts of suspended crystals to the surface whereas slowly ascending magma batches erupted free of accumulated crystals. Pulsating magma ascent rates led to mixing of magma batches in various stages of fractionation and equilibration. On average, 13 wt % of the parental melts were left behind in the conduit systems as cumulates, irregularly distributed across the mantle–crust boundary to high levels in the crust. At this early stage of the volcanism, crustal underplating would be insignificant.

The conduit systems of the Vaigat Formation have many features in common with the crystal-rich magma chambers proposed by Sinton & Detrick (1992) for mid-ocean ridges. Despite the differences in lithosphere thickness, the rifting continent in West Greenland may be viewed as a slow-spreading ridge with high magma supply rates where the large magma volumes mainly formed new crust by aggradation of the lava plateau.

ACKNOWLEDGEMENTS

We are grateful to Jørn Rønsbo for assistance with the set-up of the microprobe, particularly for the trace-element analyses, and to Christian Bender-Koch for the Mössbauer analyses of glass separates. Stefan Bernstein, Henriette Hansen and Sven Maaløe provided constructive comments and discussions, as did the reviewers Nick Arndt, Miranda Fram and Don Francis. The Arctic Station in Godhavn, and the Geological Survey of Greenland's expedition leaders Flemming G. Christiansen and Feiko Kalsbeek provided extensive support during field work. The Danish Natural Science Research Council provided the microprobe facility. Publication of this paper

is authorized by the Geological Survey of Denmark and Greenland.

REFERENCES

Aitken, B. G. & Echeverria, L. M. (1984). Petrology and geochemistry of komatiites and tholeiites from Gorgona Island, Colombia. *Contributions to Mineralogy and Petrology* **66**, 415–427.

Albarède, F. (1992). How deep do common basaltic magmas form and differentiate? *Journal of Geophysical Research* **97**(B), 10997–11009.

Albarède, F., Luais, B., Fitton, J. G., Semet, M., Kaminski, E., Upton, B. G. J., Bachelèry, P. & Cheminée, J.-L. (1997). The geochemical regimes of Piton de la Fournaise volcano (Réunion) during the last 530 000 years. *Journal of Petrology* **38**, 171–201.

Allan, J. F. (1992). Cr-spinel as a petrogenetic indicator: deducing magma composition from spinels in highly altered basalts from the Japan Sea, Sites 794 and 797. In: Tamaki, K., Suyehiro, K., Allan, J. F. & McWilliams, M. (eds) *Proceedings of the Ocean Drilling Program, Scientific Results, 127/128*. College Station, TX: Ocean Drilling Program, pp. 837–847.

Allan, J. F. (1994). Cr-rich spinel in depleted basalts from the Lau Basin backarc: petrogenetic history from Mg–Fe crystal–liquid exchange. In: Hawkins, J., Parson, L. & Allan, J. F. (eds) *Proceedings of the Ocean Drilling Program, Scientific Results, 135*. College Station, TX: Ocean Drilling Program, pp. 565–583.

Allan, J. F. & Dick, H. J. B. (1996). Cr-rich spinel as a tracer for melt migration and melt–wall rock interaction in the mantle: Hess Deep, Leg 147. In: Mével, C., Gillis, K. M., Allan, J. F. & Meyer, P. S. (eds) *Proceedings of the Ocean Drilling Program, Scientific Results, 147*. College Station, TX: Ocean Drilling Program, pp. 157–172.

Arai, S. (1994*a*). Compositional variation of olivine–chromian spinel in Mg-rich magmas as a guide to their residual spinel peridotites. *Journal of Volcanology and Geothermal Research* **59**, 279–293.

Arai, S. (1994*b*). Characterization of spinel peridotites by olivine–spinel compositional relationships: review and interpretation. *Chemical Geology* **113**, 191–204.

Ariskin, A. & Nikolaev, G. S. (1996). An empirical model for the calculation of spinel–melt equilibria in mafic igneous systems at atmospheric pressure: 1. Chromian spinels. *Contributions to Mineralogy and Petrology* **123**, 282–292.

Ariskin, A. A., Frenkel, M. Y., Barmina, G. S. & Nielsen, R. L. (1993). COMAGMAT: a FORTRAN program to model magma differentiation processes. *Computers and Geosciences* **19**, 1155–1170.

Arndt, N. T. (1986). Differentiation of komatiite flows. *Journal of Petrology* **27**, 279–301.

Arndt, N. T., Naldrett, A. J. & Pyke, D. R. (1977). Komatiitic and iron-rich tholeiitic lavas of Munro Township, northeast Ontario. *Journal of Petrology* **18**, 319–369.

Baker, M. B., Alves, S. & Stolper, E. (1996). Petrography and petrology of the Hawaii Scientific Drilling Project lavas: inferences from olivine phenocryst abundances and compositions. *Journal of Geophysical Research* **101**(B), 11715–11727.

Balhaus, C., Berry, R. F. & Green, D. H. (1991). High pressure experimental calibration of the olivine–orthopyroxene–spinel oxygen geobarometer: implications for the oxidation state of the upper mantle. *Contributions to Mineralogy and Petrology* **107**, 27–40.

Barnes, S. J. (1998). Chromite in komatiites, 1. Magmatic controls on crystallization and composition. *Journal of Petrology* **39**, 1689–1720.

Bernstein, S., Kelemen, P. B. & Brooks, C. K. (1998). Depleted spinel harzburgite xenoliths in Tertiary dykes from East Greenland: restites from high-degree melting. *Earth and Planetary Science Letters* **154**, 221–235.

Bristow, J. W. (1984). Picritic rocks of the North Lebombo and South-East Zimbabwe. In: Erlank, A. K. (ed.) *Petrogenesis of the Volcanic Rocks of the Karoo Province. Geological Society of South Africa, Special Publication* **13**, 105–123.

Campbell, I. H. & Griffiths, R. W. (1990). Implications of mantle plume structure for the evolution of flood basalts. *Earth and Planetary Science Letters* **99**, 79–93.

Campbell, I. H. & Griffiths, R. W. (1992). The changing nature of mantle hotspots through time: implications for the chemical evolution of the mantle. *Journal of Geology* **92**, 497–523.

Chalmers, J. A., Pulvertaft, T. C. R., Marcussen, C. & Pedersen, A. K. (1999). New insight into the structure of the Nuussuaq Basin, central West Greenland. *Marine and Petroleum Geology* **16**, 197–224.

Chen, C.-Y. (1993). High-magnesium primary magmas from Haleakala Volcano, east Maui, Hawaii: petrography, nickel, and major-element constraints. *Journal of Volcanology and Geothermal Research* **55**, 143–153.

Christie, D. M., Carmichael, I. S. E. & Langmuir, C. H. (1986). Oxidation states of mid-ocean ridge basalt glasses. *Earth and Planetary Science Letters* **79**, 397–411.

Clarke, D. B. (1970). Tertiary basalts of the Baffin Bay: possible primary magma from the mantle. *Contributions to Mineralogy and Petrology* **25**, 203–224.

Clarke, D. B. & O'Hara, M. J. (1979). Nickel and the existence of high-MgO liquids in nature. *Earth and Planetary Science Letters* **44**, 153–158.

Clarke, D. B. & Pedersen, A. K. (1976). Tertiary volcanic province of West Greenland. In: Escher, A. & Watt, W.S. (eds) *Geology of Greenland*. Copenhagen: Geological Survey of Greenland, pp. 364–385.

Cox, K. G. (1980). A model for flood basalt volcanism. *Journal of Petrology* **21**, 629–650.

Cox, K. G., Duncan, A. R., Bristow, J. W., Taylor, S. R. & Erlank, A. J. (1984). Petrogenesis of the basic rocks of the Lebombo. In: Erlank, A. K. (ed.) *Petrogenesis of the Volcanic Rocks of the Karoo Province. Geological Society of South Africa, Special Publication* **13**, 149–169.

Dick, H. J. B. & Bullen, T. (1984). Chromian spinel as a petrogenetic indicator in abyssal and alpine-type peridotites and spatially associated lavas. *Contributions to Mineralogy and Petrology* **86**, 54–76.

Donaldson, C. H. (1976). An experimental investigation of olivine morphology. *Contributions to Mineralogy and Petrology* **57**, 187–213.

Donaldson, C. H. & Brown, R. W. (1977). Refractory megacrysts and magnesium-rich melt inclusions within spinel in oceanic tholeiites; indicators of magma mixing and parental magma composition. *Earth and Planetary Science Letters* **37**, 81–89.

Drever, H. I. & Johnston, R. (1957). Crystal growth of forsteritic olivine in magmas and melts. *Transactions of the Royal Society of Edinburgh* **63**, 289–315.

Echeverria, L. M. (1980). Tertiary or Mesozoic komatiites from Gorgona Island, Colombia: field relations and geochemistry. *Contributions to Mineralogy and Petrology* **73**, 253–266.

Eggins, S. M. (1993). Origin and differentiation of picritic arc magmas, Ambae (Aoba), Vanuatu. *Contributions to Mineralogy and Petrology* **114**, 79–100.

Elliott, T. R., Hawkesworth, C. J. & Grönvold, K. (1991). Dynamic melting of the Iceland plume. *Nature* **351**, 201–206.

Elthon, D. & Ridley, W. I. (1979). Comments on: 'The partitioning of nickel between olivine and silicate melt' by S. R. Hart and K. E. Davis. *Earth and Planetary Science Letters* **44**, 162–164.

Escher, J. C. & Pulvertaft, T. C. R. (1995). *Geological Map of Greenland 1:2 500 000*. Copenhagen: Geological Survey of Greenland.

Ford, C. E., Russell, D. G., Craven, J. A. & Fisk, M. R. (1983). Olivine–liquid equilibria: temperature, pressure, and composition dependence of the crystal/liquid cation partition coefficients for Mg, Fe^{2+}, Ca and Mn. *Journal of Petrology* **24**, 256–265.

Fram, M. S. & Lesher, C. E. (1997). Generation and polybaric differentiation of East Greenland Early Tertiary flood basalts. *Journal of Petrology* **38**, 231–275.

Francis, D. (1985). The Baffin Bay lavas and the value of picrites as analogues of primary magmas. *Contributions to Mineralogy and Petrology* **89**, 144–154.

Francis, D. (1995). The implications of picritic lavas for the mantle sources of terrestrial volcanism. *Lithos* **34**, 89–105.

Frost, B. R. (1991). Introduction to oxygen fugacity and its petrological significance. In: Lindsley, D. H. (ed.) *Oxide Minerals: Petrologic and Magnetic Significance. Mineralogical Society of America, Reviews in Mineralogy* **25**, 1–9.

Garcia, M. O. (1996). Petrography and olivine and glass chemistry of lavas from the Hawaii Scientific Drilling Project. *Journal of Geophysical Research* **101**(B), 11701–11713.

Gill, R. C. O., Pedersen, A. K. & Larsen, J. G., (1992). Tertiary picrites in West Greenland: melting at the periphery of a plume? In: Storey, B. C., Alabaster, T. & Pankhurst, R. J. (eds) *Magmatism and the Causes of Continental Break-up. Geological Society, London, Special Publication* **68**, 335–348.

Goodrich, C. A. & Patchett, P. J. (1991). Nd and Sr isotope chemistry of metallic iron-bearing, sediment-contaminated Tertiary volcanics from Disko Island, Greenland. *Lithos* **27**, 13–27.

Gurenko, A. A., Hansteen, T. H. & Schmincke, H.-U. (1996). Evolution of parental magmas of Miocene shield basalts of Gran Canaria (Canary Islands): constraints from crystal, melt and fluid inclusions in minerals. *Contributions to Mineralogy and Petrology* **89**, 422–435.

Haggerty, S. E. (1976). Opaque mineral oxides in terrestrial igneous rocks. In: Rumble, D. (ed.) *Oxide Minerals. Mineralogical Society of America, Reviews in Mineralogy* **3**, Hg101–Hg300.

Haggerty, S. E. (1991). Oxide mineralogy of the upper mantle. In: Lindsley, D. H. (ed.) *Oxide Minerals: Petrologic and Magnetic Significance. Mineralogical Society of America, Reviews in Mineralogy* **25**, 355–416.

Hansen, H. & Nielsen, T. F. D. (1999). Crustal contamination in Palaeogene East Greenland flood basalts: plumbing system evolution during continental rifting. *Chemical Geology* **157**, 89–118.

Hanson, B. & Jones, J. H. (1998). The systematics of Cr^{3+} and Cr^{2+} partitioning between olivine and liquid in the presence of spinel. *American Mineralogist* **83**, 669–684.

Hart, S. R. & Davis, K. E. (1978). Nickel partitioning between olivine and silicate melt. *Earth and Planetary Science Letters* **40**, 203–219.

Hart, S. R. & Davis, K. E. (1979). Reply to D. B. Clarke and M. J. O'Hara, 'Nickel and the existence of high-MgO liquids in nature'. *Earth and Planetary Science Letters* **44**, 159–161.

Helz, R. T. (1987). Diverse olivine types in lava of the 1959 eruption of Kilauea volcano and their bearing on eruption dynamics. *US Geological Survey, Professional Paper* **1350**, 691–722.

Herzberg, C. (1995). Generation of plume magmas through time: an experimental perspective. *Chemical Geology* **126**, 1–16.

Herzberg, C. & O'Hara, M. J. (1998). Phase equilibrium constraints on the origin of basalts, picrites, and komatiites. *Earth-Science Reviews* **44**, 39–79.

Herzberg, C. & Zhang, J. (1996). Melting experiments on anhydrous peridotite KLB-1: compositions of magmas in the upper mantle and transition zone. *Journal of Geophysical Research* **101**(B), 8271–8295.

Hill, R. I. (1991). Starting plumes and continental break-up. *Earth and Planetary Science Letters* **104**, 398–416.

Holm, P. M., Gill, R. C. O., Pedersen, A. K., Larsen, J. G., Hald, N., Nielsen, T. F. D. & Thirlwall, M. F. (1993). The Tertiary picrites of West Greenland: contributions from 'Icelandic' and other sources. *Earth and Planetary Science Letters* **115**, 227–244.

Jurewich, A. J. G. & Watson, E. B. (1988). Cations in olivine, part 1: Calcium partitioning and calcium–magnesium distribution between olivines and coexisting melts, with petrological applications. *Contributions to Mineralogy and Petrology* **99**, 176–185.

Kamenetsky, V., Métrich, N. & Cioni, R. (1995*a*). Potassic primary melts of Vulsini (Roman Province): evidence from mineralogy and melt inclusions. *Contributions to Mineralogy and Petrology* **120**, 186–196.

Kamenetsky, V., Sobolev, A. V., Joron, J.-L. & Semet, M. P. (1995*b*). Petrology and geochemistry of Cretaceous ultramafic volcanics from eastern Kamchatka. *Journal of Petrology* **36**, 637–662.

Kamenetsky, V. S., Eggins, S. M., Crawford, A. J., Green, D. H., Gasparon, M. & Falloon, T. J. (1998). Calcic melt inclusions in primitive olivine at 43°N MAR: evidence for melt–rock reaction/melting involving clinopyroxene-rich lithologies during MORB generation. *Earth and Planetary Science Letters* **160**, 115–132.

Kent, A. J. R., Stolper, E. M., Woodhead, J., Hutcheon, I. D. & Francis, D. (1998). Using glass inclusions to investigate a heterogeneous mantle: an example from N- and EMORB-like lavas from Baffin Island. *Mineralogical Magazine* **62A**(Goldschmidt Conference), 765–766.

Kilinc, A., Carmichael, I. S. E., Rivers, M. L. & Sack, R. O. (1983). The ferric–ferrous ratio of natural silicate liquids equilibrated in air. *Contributions to Mineralogy and Petrology* **83**, 136–140.

Krishnamurthy, P. & Cox, K. G. (1977). Picrite basalts and related lavas from the Deccan traps of Western India. *Contributions to Mineralogy and Petrology* **62**, 53–75.

Langmuir, C. H., Klein, E. M. & Plank, T. (1992). Petrological systematics of mid-ocean ridge basalts: constraints on melt generation beneath ocean ridges. In: Phipps Morgan, J., Blackman, D. K. & Sinton, J. M. (eds) *Mantle Flow and Melt Generation at Mid-ocean Ridges. Geophysical Monograph, American Geophysical Union* **71**, 183–280.

Le Bas, M. J. (ed.) (2000). *A Classification of Igneous Rocks and Glossary of Terms. Recommendations of the IUGS Subcommission on the Systematics of Igneous Rocks*, 2nd edn. Oxford: Blackwell Scientific (in press).

Lesher, C. M. (1989). Komatiite-associated nickel sulfide deposits. In: Whitney, J. A. & Naldrett, A. J. (eds) *Ore Deposition Associated with Magmas. Reviews in Economic Geology* **4**, 45–101.

Li, J.-P., O'Neil, H. St C. & Seifert, F. (1995). Subsolidus phase relations in the system $MgO–SiO_2–Cr–O$ in equilibrium with metallic Cr, and their significance for the petrochemistry of chromium. *Journal of Petrology* **36**, 107–132.

Lightfoot, P. C., Hawkesworth, C. J., Olshevsky, K., Green, A., Doherty, W. & Keays, R. R. (1997). Geochemistry of Tertiary tholeiites and picrites from Qeqertarssuaq (Disko Island) and Nuussuaq, West Greenland with implications for the mineral potential of comagmatic intrusions. *Contributions to Mineralogy and Petrology* **128**, 139–163.

Maaløe, S. (1973). Temperature and pressure relations of ascending primary magmas. *Journal of Geophysical Research* **78**, 6877–6886.

Maaløe, S. (1979). Compositional range of primary tholeiitic magmas evaluated from major-element trends. *Lithos* **12**, 59–72.

Maaløe, S. & Hansen, B. (1982). Olivine phenocrysts of Hawaiian olivine tholeiite and oceanite. *Contributions to Mineralogy and Petrology* **81**, 203–211.

Maaløe, S., Tumyr, O. & James, D. (1989). Population density and zoning of olivine phenocrysts in tholeiites from Kauai, Hawaii. *Contributions to Mineralogy and Petrology* **101**, 176–186.

Maurel, C. & Maurel, P. (1982). Étude expérimentale de l'équilibre Fe^{2+}–Fe^{3+} dans les spinelles chromifères et les liquides silicatés basiques coexistants, à 1 atm. *Comptes Rendus de l'Académie des Sciences* **295**, 209–212.

McKenzie, D. & Bickle, M. J. (1988). The volume and composition of melt generated by extension of the lithosphere. *Journal of Petrology* **29**, 625–679.

Melluso, L., Beccaluva, L., Brotzu, P., Gregnanin, A., Gupta, A. K., Morbidelli, L. & Traversa, G. (1995). Constraints on the mantle sources of the Deccan Traps from the petrology and geochemistry of the basalts of Gujarat State (western India). *Journal of Petrology* **36**, 1393–1432.

Murck, B. W. & Campbell, I. H. (1986). The effects of temperature, oxygen fugacity and melt composition on the behaviour of chromium in basic and ultrabasic melts. *Geochimica et Cosmochimica Acta* **50**, 1871–1887.

Nielsen, T. F. D., Soper, N. J., Brooks, C. K., Faller, A. M., Higgins, A. C. & Matthews, D. W. (1981). The pre-basaltic sediments and the Lower Basalts at Kangerdlugssuaq, East Greenland: their stratigraphy, lithology, palaeomagnetism and petrology. *Meddelelser om Grønland, Geoscience* **6**, 28 pp.

Nisbet, E. G., Cheadle, M. J., Arndt, N. T. & Bickle, M. J. (1993). Constraining the potential temperature of the Archaean mantle: a review of the evidence from komatiites. *Lithos* **30**, 291–307.

Nisbet, E. G., Bickle, M. J. & Martin, A. (1977). The mafic and ultramafic lavas of the Belingwe greenstone belt, Rhodesia. *Journal of Petrology* **18**, 521–566.

Pearce, T. H. (1984). The analysis of zoning in magmatic crystals with emphasis on olivine. *Contributions to Mineralogy and Petrology* **86**, 149–154.

Pedersen, A. K. (1979*a*). A shale buchite xenolith with armalcolite and native iron in a lava from Asuk, Disko, central West Greenland. *Contributions to Mineralogy and Petrology* **69**, 83–94.

Pedersen, A. K. (1979*b*). Basaltic glass with high-temperature equilibrated immiscible sulphide bodies with native iron from Disko, central West Greenland. *Contributions to Mineralogy and Petrology* **69**, 397–407.

Pedersen, A. K. (1985). Reaction between picrite magma and continental crust: early Tertiary silicic basalts and magnesian andesites from Disko, West Greenland. *Bulletin Grønlands Geologiske Undersøgelse* **152**, 126 pp.

Pedersen, A. K. & Pedersen, S. (1987). Sr isotope chemistry of contaminated Tertiary volcanic rocks from Disko, central West Greenland. *Bulletin of the Geological Society of Denmark* **36**, 315–336.

Pedersen, A. K., Larsen, L. M. & Dueholm, K. S. (1993). Geological section along the south coast of Nuussuaq, central West Greenland, 1:20 000 Coloured Geological Sheet. Copenhagen: Geological Survey of Greenland.

Pedersen, A. K., Larsen, L. M., Pedersen, G. K. & Dueholm, K. S. (1996). Filling and plugging of a marine basin by volcanic rocks: the Tunoqqu Member of the Lower Tertiary Vaigat Formation on Nuussuaq, central West Greenland. *Bulletin Grønlands Geologiske Undersøgelse* **171**, 5–28.

Pedersen, G. K., Larsen, L. M., Pedersen, A. K. & Hjortkjær, B. F. (1998). The synvolcanic Naajaat lake, Paleocene of West Greenland. *Palaeogeography, Palaeoclimatology, Palaeoecology* **140**, 271–287.

Roeder, P. L. & Emslie, R. F. (1970). Olivine–liquid equilibrium. *Contributions to Mineralogy and Petrology* **29**, 275–289.

Saunders, A. D., Fitton, J. G., Kerr, A. C., Norry, M. J. & Kent, R. W. (1997). The North Atlantic Igneous Province. In: Mahoney, J. J. & Coffin, M. L. (eds) *Large Igneous Provinces. Geophysical Monograph, American Geophysical Union* **100**, 45–93.

Sinton, J. M. & Detrick, R. S. (1992). Mid-ocean ridge magma chambers. *Journal of Geophysical Research* **97**(B), 197–216.

Sobolev, A. V. & Nikogosian, I. K. (1994). Petrology of long-lived mantle plume magmatism: Hawaii, Pacific, and Reunion Island, Indian Ocean. *Petrology* **2**, 111–144.

Sobolev, A. V. & Shimizu, N. (1994). The origin of typical N-MORB: the evidence from a melt inclusions study. *Mineralogical Magazine* **58A**, 862–863.

Storey, M., Duncan, R. A., Pedersen, A. K., Larsen, L. M. & Larsen, H. C. (1998). $^{40}Ar/^{39}Ar$ geochronology of the West Greenland Tertiary volcanic province. *Earth and Planetary Science Letters* **160**, 569–586.

Ulmer, P. (1989). The dependence of the Fe^{2+}–Mg cations-partitioning between olivine and basaltic liquid on pressure, temperature and composition. An experimental study to 30 kbars. *Contributions to Mineralogy and Petrology* **101**, 261–273.

Upton, B. G. J. (1988). History of Tertiary igneous activity in the N Atlantic borderlands. In: Morton, A. C. & Parson, L. M. (eds) *Early Tertiary Volcanism and the Opening of the NE Atlantic. Geological Society, London, Special Publication* **39**, 429–453.

White, R. & McKenzie, D. (1989). Magmatism at rift zones: the generation of volcanic continental margins and flood basalts. *Journal of Geophysical Research* **94**(B), 7685–7729.

Yang, H.-J., Frey, F., Garcia, M. O. & Clague, D. A. (1994). Submarine lavas from Mauna Kea volcano, Hawaii: implications for Hawaiian shield stage processes. *Journal of Geophysical Research* **99**(B), 15577–15594.

Zhou, M.-F. & Kerrich, R. (1992). Morphology and composition of chromite in komatiites from the Belingwe greenstone belt, Zimbabwe. *Canadian Mineralogist* **30**, 303–317.

APPENDIX: SAMPLE DATA, VAIGAT FORMATION, WEST GREENLAND

Sample*	Long. W	Lat. N	Area	Member†	Lithol.‡	Oliv.§	Crm.§	Glass	Other¶
136943	53°24′18″	70°11′28″	N Disko	Ord	pic-br	**x**	**x**	x	glass incl.
156737	53°06′14″	70°05′35″	N Disko	Ord	pic-br	**x**	**x**	x	
176712	53°36′43″	70°05′27″	N Disko	Ord	pic-br			x	
264099	53°32′04″	70°04′28″	N Disko	Ord	pic-br			x	
264105	53°31′08″	70°04′15″	N Disko	Ord	pic-br	**x**		x	
264137	53°30′53″	70°04′10″	N Disko	Ord	pic-br	x	x	x	
264217	53°41′20″	70°23′00″	Nuussuaq	Nau	pic-br	x		x	
264219	53°38′34″	70°22′40″	Nuussuaq	Nau	pic-br			x	
327100	53°23′05″	70°11′00″	N Disko	Ord	pic-br	**x**	**x**	x	
332771	53°59′10″	70°35′13″	Nuussuaq	Nau	pic-br	**x**	**x**	x	glass incl.
362148	53°18′03″	70°22′10″	Nuussuaq	Nau	pic-br	**x**	**x**	x	glass incl.
400450	54°10′27″	70°31′10″	Nuussuaq	Ana	pic-br	**x**	x	x	
400452	54°13′08″	70°32′12″	Nuussuaq	Ana	pic-br	**x**	**x**	x	glass incl.
400493	54°03′10″	70°32′05″	Nuussuaq	Ana	bas-br		x	x	plag + cpx

*All sample numbers are GGU numbers.
†Volcanic members: Ana, Anaanaa Mb; Nau, Naujánguit Mb; Ord, Ordlingassoq Mb.
‡Lithologies: pic, picrite; bas, basalt; br, pillow breccia.
§x, analysed; **x**, the analyses comprise olivine with *mg*-number >90, or chromite in such olivines.
¶Other analysed phases. Incl., inclusions; plag, plagioclase; cpx, clinopyroxene.